To the Graduate Council:

I am submitting herewith a dissertation written by Zia Allen Faiz Tompkins entitled “A Methodology for Establishing Zones of Acceptable CAAS Coverage for a New Storage Facility Utilizing MCNP 5 in Adjoint.” I have examined the final electronic copy of this thesis for form and content and recommend that it be accepted in partial fulfillment of the requirements for the degree of Master of Science, with a major in Nuclear Engineering.

Ronald Pevey, Major Professor

We have read this thesis
and recommend its acceptance:

Lawrence Miller

Lawrence Townsend

Accepted for the Council:

Carolyn R. Hodges
Vice Provost and Dean of the Graduate School

(Original signatures are on file with official student records.)

A Methodology for Establishing Zones of Acceptable CAAS Coverage for a New Storage Facility Utilizing MCNP 5 in Adjoint

A Thesis

Presented for the

Master of Science

Degree

The University of Tennessee, Knoxville

Zia Tompkins

August 2008

Copyright © 2008 by Zia Tompkins
All rights reserved.

DEDICATION

This work is dedicated to all those who would sacrifice a lifetime of toil for the dream of one day being cited.

ACKNOWLEDGEMENTS

I'd first like to thank Dr. Peter Angelo of Y-12 NSC of whom this project is his brainchild. Furthermore I'd like to thank my faculty advisor Dr. Ronald Pevey of the University of Tennessee for his crucial advice and guidance during this long journey. I'd also like to thank my committee members Dr. Lawrence Townsend and Dr. Laurence Miller for their time in reviewing this thesis along with the rest of the Department of Nuclear Engineering at the University Tennessee for their unerring support. Finally I'd like to thank my mom, Saeeda, my little sister, Gladys and my girlfriend, Crystal, whose constant encouragement and patience has made this work possible.

ABSTRACT

ANSI/ANS 8.3 “Criticality Accident Alarm System”, Appendix B states “Determining the adequacy of criticality alarm detector placement is far from an exact process”. With this statement in mind a novel method for establishing areas of acceptable Criticality Accident Alarm System (CAAS) coverage was developed and demonstrated utilizing Los Alamos’ Monte Carlo N-Particle Code 5 (MCNP5) in multigroup Adjoint. Validation of the methodology was shown in the comparison of benchmark calculations with empirical results of Sandia testing and with hand calculations utilizing ANS 8.3. Demonstration involved the determination of zones of CAAS coverage from detector sensitivity maps generated by MCNP5 for a conceptual geometry of a new storage facility involving homogenized concrete and BoroBond® slabs. Multiple detector coverage was further demonstrated through the superimposing of several maps corresponding to differing detector locations.

TABLE OF CONTENTS

Chapter Page

CHAPTER I ... 1
Motivation, Introduction and Scope ... 1
Criticality Accident Alarm Systems at Y-12 NSC ... 1
Detector Sensitivity via Monte Carlo in Adjoint ... 3
CHAPTER II ... 5
Theoretical Background ... 5
The Transport Equation in Adjoint ... 5
The Monte Carlo Method ... 9
Monte Carlo in Adjoint ... 12
CHAPTER III ... 14
Techniques and Codes ... 14
MCNP 5 ... 14
MCNP 5 in Adjoint ... 16
Data Post-Processing ... 20
Benchmarking and Validation ... 22
The Benchmark Example ... 22
Source Spectra ... 23
Dose Rate Response Function ... 23
Source Strength Calculation ... 23
Benchmark Results ... 24
Validation ... 26
CHAPTER V ... 30
Conceptual Storage Facility Example Problem ... 30
The Example Storage Facility ... 30
RCSB Configuration ... 31
Example Problem Setup ... 32
Example Problem Results ... 32
CHAPTER VI ... 38
Multiple Detector Coverage ... 38
CHAPTER VII ... 39
Conclusions and Recommendations ... 39
LIST OF REFERENCES ... 40
APPENDICES ... 42
APPENDIX A ... 43
APPENDIX B ... 44
APPENDIX C ... 46
Vita ... 50

LIST OF FIGURES

Figure Page

Figure 1. Present Y-12 CAAS Detector Coverage Scheme 1
Figure 2. CIDAS® 3-Train Loop System 2
Figure 3. Ludwig Boltzmann, Norbert Weiner and Enrico Fermi 5
Figure 4. Stanisław Ulam 10
Figure 5. The Random Walk 10
Figure 6. Mesh Grid Tally Superimposed on Annular Geometry 15
Figure 7. MCNP5 MGXSNP Multigroup Structure 17
Figure 8. Calculation of Normalization Weighting Factor 19
Figure 9. Benchmark Example Geometry 22
Figure 10. Source Strength Calculation of Neutrons and Photons with WGT=1 25
Figure 11. Benchmark Forward Calculation, Neutrons and Photons 25
Figure 12. Benchmark Forward Dose Map (0.333 rad/s contour) 25
Figure 13. Benchmark Adjoint Calculation, Neutrons and Photons 25
Figure 14. Benchmark Adjoint Dose Map (0.333 rad/s contour) 28
Figure 15. Bench Detector Sensitivity Map, 1.4 x 10^{-9} rad/s Contour 28
Figure 16. Adjoint Calculation vs. Empirical vs. ANS 8.3 Analytical 38
Figure 17. Example Storage Facility 29
Figure 18. The Rackable Can Storage Box 30
Figure 19. Example Storage Facility w/ 40 RCSB's 31
Figure 20. Example Storage Facility Dose Rate Map 32
Figure 21. Example Storage Facility Forward Calculation, Neutrons and Photons 32
Figure 22. Example Storage Facility Adjoint Calculation, Neutrons and Photons 34
Figure 23. Example Detector 1 Sensitivity Map, 1.4 x 10^{-9} rad/s Contour 34
Figure 24. Example Detector 2 Sensitivity Map, 1.4 x 10^{-9} rad/s Contour 35
Figure 25. Example Detector 3 Sensitivity Map, 1.4 x 10^{-9} rad/s Contour 35
Figure 26. Triple-Detector Coverage Sensitivity Map, 1.4 x 10^{-9} rad/s Contour 36

CHAPTER I
MOTIVATION, INTRODUCTION AND SCOPE

Criticality Accident Alarm Systems at Y-12 NSC

Currently, criticality accident alarm systems (CAAS) are designed to meet the American National Standards Institute (ANSI) / American Nuclear Society (ANS) Standard 8.3 (1997)[7]. This standard mandates the ability of a CAAS to detect a minimum accident of concern, defined to be that which causes an absorbed dose rate in air of 20 rad/min at 2 meters from the reacting material. To comply with this requirement, the Y-12 National Security Complex (NSC) has since 1958, employed a series of fixed detector stations each consisting of two plastic scintillators. Using a response rate of 30 mrad/hr, early Sandia testing revealed a detection range of these detectors to be 400 ft with nominal shielding[2]. This value was then translated into a 400 ft radius circular region. Acceptable areas of CAAS coverage at Y-12 NSC are defined as the minimum overlap of two of these circular regions as shown in Figure 1. As a consequence, all fissile material operations are prohibited outside of these overlapping regions.[2]

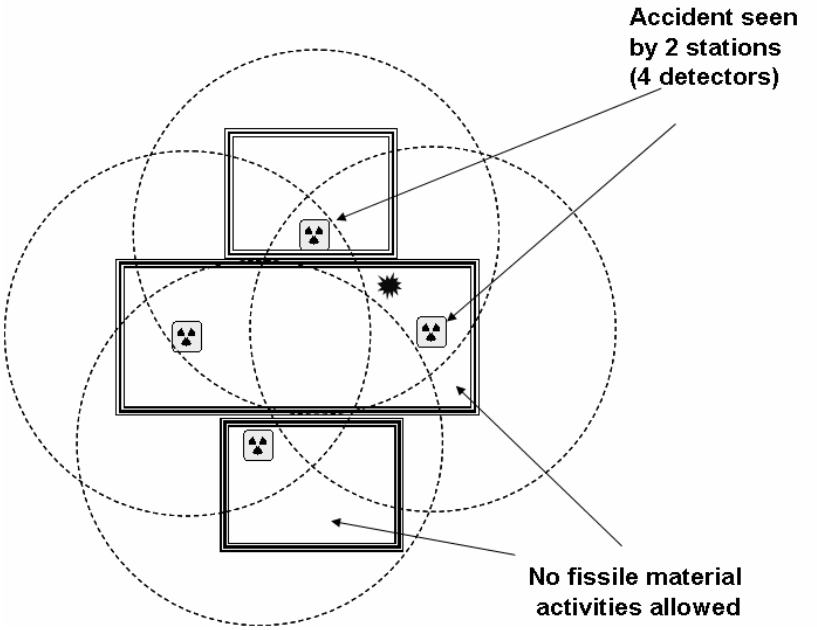


Figure 1: Present Y-12 CAAS Detector Coverage Scheme

While this method allows for simplicity in detector deployment it also ignores the particular geometric and material characteristics in the vicinity of coverage. Depending on specifics, this may lead to an overly conservative arrangement unduly limiting areas of fissile material operation, or conversely, lead to an unsafe condition regarding CAAS effectiveness.

With the development of new storage facilities underway, a new detector arrangement scheme involving CIDAS® loop detectors is being implemented.[2] The system is made up of three independent serially-linked loops, or *trains*, of up to 50 detectors each, operating under a 2/3 voting logic as shown in Figure 2. Thus with a detector set point of 100 mrad/hour, if detectors from two of the three loops detect the accident, the alarm is tripped. This increases redundancy and reduces false alarms.[2]

This new CAAS arrangement however, necessitates a new detector placement methodology to supplant the current overlapping-circle format. This improved methodology must take into account the geometry and composition within the detector's zone of coverage and yield a minimum accident detectablity contour much more physically representative of what the detector actually sees than that given by the circle scheme. Subsequently this will permit more space for fissile material operations within a new storage facility while improving safety. The development and demonstration of this methodology is the scope of this paper.

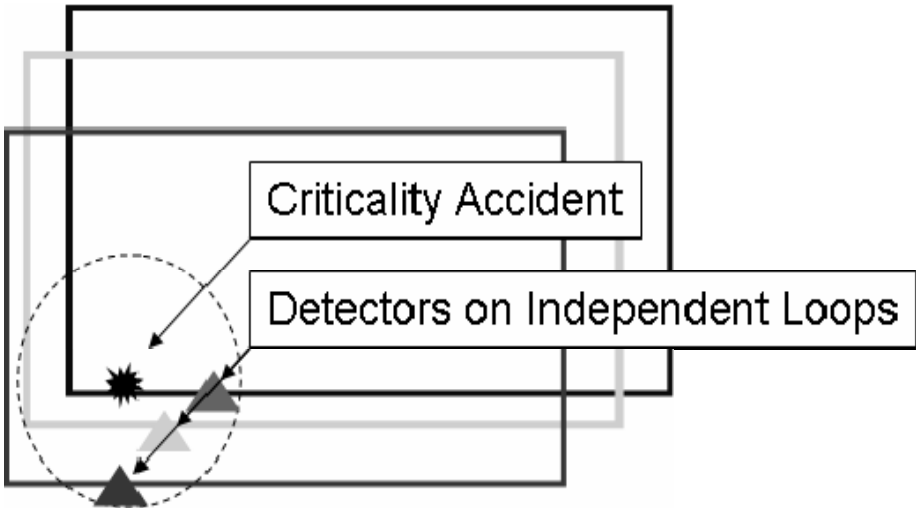


Figure 2: CIDAS® 3-Train Loop System

Detector Sensitivity via Monte Carlo in Adjoint

One technique for determining the sensitivity of a detector in a particular system is through a Monte Carlo simulation. Beginning with a basic facility geometry with a representative composition, a model is created within a Monte Carlo code. A point source, representing a possible accident, is then added with an appropriate source strength and spectrum at a likely location. A dose rate response curve is subsequently associated with a mesh grid tally spanning the model geometry. As the forward simulation is run the particle transport produces a dose map of the vicinity. Worst case locations for detector placement appear as areas of low dose rate in the dose map, as these represent areas where fewer accident particles reach. Placing detectors in those locations may be necessary for complete CAAS coverage of an area even though they represent areas of decreased transport. Use of forward calculations to determine the sensitivity of a given detector to accidents at various locations requires multiple calculations, each of which places the accident source at a different location—usually on a regular grid that can then be translated into a detector sensitivity map for the specified detector, indicating what source locations the detector can "see".

If the detector is modeled as a point flux tally with an appropriate response function, the simulation can be run in adjoint with the point detector serving as the adjoint source and, again, with a mesh grid tally. This process produces the detector sensitivity map for the specified detector in a single transport calculation, saving large amounts of computer time. Once the necessary contour corresponding to the minimum accident of concern detectablity based on detector setpoint (particle detection rate) is plotted, the areas of allowable safe activity within the detector's zone of coverage are established. As an added benefit, the use of a point source and point detector allows the forward and adjoint calculations for a given situation to check each other. This is due to the requirement that the adjoint result at the forward source location should agree with the forward result at the adjoint detector location. These adjoint calculations can then easily be repeated for different detector locations until ideal CAAS coverage is found. Multiple detector coverage can then be further

demonstrated through the superposition of these results for several detectors. Utilizing Monte Carlo in this manner will be the focus of this project in establishing the CAAS coverage.

CHAPTER II
THEORETICAL BACKGROUND

The Transport Equation in Adjoint

The foundations of transport theory were laid down in the 19th century with Ludwig Boltzmann's kinetic theory of gases. The field later came into its own in the 1930's with the study of radiation transport in stellar atmospheres and put on a solid mathematical footing by the contributions of Norbert Weiner and others. Particular interest in neutral particle transport exploded with the establishment of the first nuclear chain reaction by Enrico Fermi in 1942 as part of the Manhattan Project.

Development of a theoretical treatment of neutral particle transport usually begins with several underlying assumptions:

1. Particles are points and behave classically;
2. Particles travel in straight lines between collisions;
3. There are no inter-particle interactions;
4. Collisions are resolved instantaneously at the point of interaction;
5. Material properties are isotropic;
6. Material compositions/properties are known and time-independent; and
7. Only mean values of particle distributions are considered.

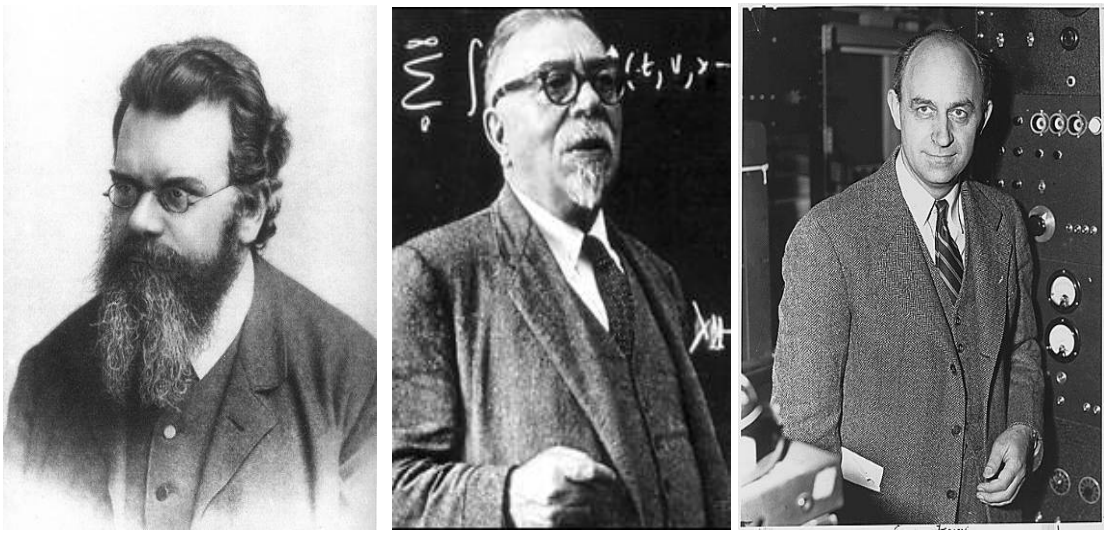


Figure 3: Ludwig Boltzmann, Norbert Weiner and Enrico Fermi

With these in hand we begin by reducing the series of complex quantum field theory (QFT) interactions that take place between particles down to a set of probabilities and interpret these as finite areas, or microscopic interaction cross sections. Microscopic cross sectional measurements have historically been expressed in units of either cm^2 or the *barn* with 1 barn = 10^{-24} cm^2. The macroscopic cross section, or simply *cross section*, $\sigma(\vec{r},E)$ is then defined as the product of the microscopic cross section with the constituent material's atom density (usually expressed in the convenient unit atoms/barn/cm), resulting in cross section units of cm^{-1}. These cross sections are a function of position, $\vec{r}$ and energy, E and represent the probability of interaction per centimeter of travel. We then define a source function $q(\vec{r},\hat{\Omega},E,t)$, which has the additional parameters of unit solid angle, $\hat{\Omega}$ and time, comprising all particles emitted through external sources, scatter or fission. We can now state an equation that will allow us to solve for the desired neutral particle flux, $\psi(\vec{r},\hat{\Omega},E,t)$ as a function of position, direction, energy and time:

$$\frac{1}{\upsilon}\frac{\partial}{\partial t}\psi(\vec{r},\hat{\Omega},E,t)+\hat{\Omega}\cdot\vec{\nabla}\psi(\vec{r},\hat{\Omega},E,t)+\sigma(\vec{r},E)\psi(\vec{r},\hat{\Omega},E,t)=q(\vec{r},\hat{\Omega},E,t) \qquad (1)$$

Equation (1) is the time-dependant Boltzmann equation.

Although a large number of transport problems of interest have explicit time-dependence, the analyses of interest in this report are at steady state. If we let the partial time derivative go to zero and the time parameter vanish, we arrive at;

$$\hat{\Omega}\cdot\vec{\nabla}\psi(\vec{r},\hat{\Omega},E)+\sigma(\vec{r},E)\psi(\vec{r},\hat{\Omega},E)=q(\vec{r},\hat{\Omega},E), \qquad (2)$$

the time-independent Boltzmann equation. We can then separate out the external source term, $q_{ex}(\vec{r},\hat{\Omega},t)$ from $q(\vec{r},\hat{\Omega},E)$ and break down the remaining flux dependant sources into those due to fission or in-scattering from other energies and directions (denoted by a prime, '). These terms are found by multiplying the time-independent directional flux $\psi(\vec{r},\hat{\Omega}',E')$ by the fission and scatter cross sections $\sigma_f(\vec{r},E)$ and $\sigma_s(\vec{r},\hat{\Omega}'\cdot\hat{\Omega},E'\rightarrow E)$. Fission is converted to a fission neutron source by including the standard fission neutron energy distribution, $\chi(E)$, and the average

number of neutrons per fission, $\upsilon(E)$. These products are then integrated over energy and direction yielding the relation[6]:

$$\begin{aligned} q(\vec{r},\hat{\Omega},E) = {} & q_{ex}(\vec{r},\hat{\Omega},E) + \\ & + \int_0^\infty dE' \int_{4\pi} d\Omega' \sigma_s(\vec{r},\hat{\Omega}'\cdot\hat{\Omega},E'\to E)\psi(\vec{r},\hat{\Omega}',E') + \\ & + \chi(E)\int_0^\infty dE' \int_{4\pi} d\Omega' \upsilon\sigma_f(\vec{r},E')\psi(\vec{r},\hat{\Omega}',E') \end{aligned} \tag{3}$$

Since we will use this equation for a detector problem without fission we will assume for now a non-multiplying system with $\sigma_f(\vec{r},E)$=0, eliminating the last integral in (3). The remaining terms are then substituted for $q(\vec{r},\hat{\Omega},E)$ in Equation (2) and re-arranged to arrive at:

$$\left[\hat{\Omega}\cdot\vec{\nabla}+\sigma(\vec{r},E)\right]\psi(\vec{r},\hat{\Omega},E) = q_{ex}(\vec{r},\hat{\Omega},E) + \int_0^\infty dE' \int_{4\pi} d\Omega' \sigma_s(\vec{r},\hat{\Omega}'\cdot\hat{\Omega},E'\to E)\psi(\vec{r},\hat{\Omega}',E') \tag{4}$$

From this form of the non-multiplying time-independent transport equation we may then define the transport operator, *H*, as an operator that transforms a function, $\zeta(\vec{r},\hat{\Omega},E)$ by the rule:

$$H\zeta = \left[\hat{\Omega}\cdot\vec{\nabla}+\sigma(\vec{r},E)\right]\zeta(\vec{r},\hat{\Omega},E) - \int dE' \int d\Omega' \sigma_s(\vec{r},\hat{\Omega}'\cdot\hat{\Omega},E'\to E)\zeta(\vec{r},\hat{\Omega}',E') \tag{5}$$

At this point it's helpful to introduce the following bracket notation denoting integration over all applicable phase space:

$$\langle a,b\rangle = \int dV \int d\Omega \int dE\, a(\vec{r},\hat{\Omega},E)\, b(\vec{r},\hat{\Omega},E) \tag{6}$$

The adjoint (†) of the operator *H*, $H^\dagger$ is then defined by the following relation:

$$\langle \zeta^\dagger, H\zeta\rangle = \langle \zeta, H^\dagger\zeta^\dagger\rangle \tag{7}$$

By substituting our definition of $H\zeta$ from Equation (5), Equation (7) can be solved (with properly chosen boundary conditions) for the adjoint transport operator rule, $H^\dagger\zeta^\dagger$:

$$H^\dagger\zeta^\dagger = \left[-\hat{\Omega}\cdot\vec{\nabla}+\sigma(\vec{r},E)\right]\zeta^\dagger(\vec{r},\hat{\Omega},E) - \int dE' \int d\Omega' \sigma_s(\vec{r},\hat{\Omega}'\cdot\hat{\Omega},E\to E')\zeta^\dagger(\vec{r},\hat{\Omega}',E') \tag{8}$$

We can then define two problems, a forward transport problem;

$$H\psi(\vec{r},\hat{\Omega},E) = S(\vec{r},\hat{\Omega},E) \tag{9}$$

and an adjoint transport problem:

$$H^{\dagger}\psi^{\dagger}\left(\vec{r},\hat{\Omega},E\right)=R\left(\vec{r},\hat{\Omega},E\right) \tag{10}$$

where $S\left(\vec{r},\hat{\Omega},E\right)$ is a known source $q_{ex}\left(\vec{r},\hat{\Omega},t\right)$ and $R\left(\vec{r},\hat{\Omega},E\right)$ is a known detector response function. Multiplying Equation (9) by $\psi^{\dagger}\left(\vec{r},\hat{\Omega},E\right)$ and Equation (10) by $\psi\left(\vec{r},\hat{\Omega},E\right)$ then integrating both over all phase space, we can subtract the resulting equations to arrive at the following relation:

$$\left\langle \psi^{\dagger},H\psi\right\rangle -\left\langle \psi,H^{\dagger}\psi^{\dagger}\right\rangle =\left\langle \psi^{\dagger},S\left(\vec{r},\hat{\Omega},E\right)\right\rangle -\left\langle \psi,R\left(\vec{r},\hat{\Omega},E\right)\right\rangle \tag{11}$$

Then recognizing the identity defined in Equation (7), the left-hand side of Equation (11) goes to zero and we are left with:

$$\left\langle \psi,R\left(\vec{r},\hat{\Omega},E\right)\right\rangle =\left\langle \psi^{\dagger},S\left(\vec{r},\hat{\Omega},E\right)\right\rangle =R \tag{12}$$

This statement implies that once the forward flux $\psi\left(\vec{r},\hat{\Omega},E\right)$ or adjoint flux $\psi^{\dagger}\left(\vec{r},\hat{\Omega},E\right)$ is known, it becomes simply a matter of performing a single integration to arrive at a common detector response, *R*.

The usefulness of Equation (12) can be illustrated using the most common situation, in which both the source and detectors can be accurately modeled with unchanging directional and energy dependence $\widetilde{S}\left(\hat{\Omega},E\right)$, $\widetilde{R}\left(\hat{\Omega},E\right)$ (which depends on their material makeup and geometrical arrangement), but can be moved around in the field to various positions (assumed to be points) $\delta\left(\vec{r}-\vec{r}_{S}\right)$ and $\delta\left(\vec{r}-\vec{r}_{D}\right)$. With this approximation, the definitions of the source and response terms become:

$$\begin{aligned} R\left(\vec{r},\hat{\Omega},E\right)&=\widetilde{R}\left(\hat{\Omega},E\right)\delta\left(\vec{r}-\vec{r}_{D}\right)\\ S\left(\vec{r},\hat{\Omega},E\right)&=\widetilde{S}\left(\hat{\Omega},E\right)\delta\left(\vec{r}-\vec{r}_{S}\right)\end{aligned} \tag{13}$$

Inserting each of these (one at a time) into Equation 12 gives us the two relationships;

$$\begin{aligned} R\left(\vec{r}_{D}\right)&=\left\langle \psi,\widetilde{R}\left(\hat{\Omega},E\right)\right\rangle_{\hat{\Omega},E}\\ R\left(\vec{r}_{S}\right)&=\left\langle \psi^{\dagger},\widetilde{S}\left(\hat{\Omega},E\right)\right\rangle_{\hat{\Omega},E}\end{aligned} \tag{14}$$

where $\left\langle a,b\right\rangle_{\hat{\Omega},E}$ denotes integration over only direction and energy.

The resulting spatial function $R(\vec{r}_D)$ is called a *dose map* or *dose rate map* and represents an extremely useful picture of doses across the geometry of a problem as a function of detector placement (with a fixed-position source). Likewise, the spatial function $R(\vec{r}_S)$ is known as a *detector sensitivity map*, a geometric picture of what a detector actually "sees" as a function of source placement (with a fixed-position detector). Both of these "maps" represent important properties of a radiation field that we will exploit going forward in establishing areas of CAAS coverage.

It is important to note one last feature of Equation (12). If the source and detector positions are fixed, then the value of $R(\vec{r}_S)$ at the fixed source position and that of $R(\vec{r}_D)$ at the fixed detector location should be the same. This requirement will become an important check for legitimacy on whatever technique is chosen to solve for *R*.

The task now becomes, if the response function $R(\vec{r},\hat{\Omega},E)$ and the source distribution $S(\vec{r},\hat{\Omega},E)$ are known, how do we go about solving for the fluxes $\psi(\vec{r},\hat{\Omega},E)$ and $\psi^{\dagger}(\vec{r},\hat{\Omega},E)$ to arrive at *R*?

The Monte Carlo Method

Rather then attempting to discretize and directly solve numerically the forward and adjoint flux over the problem geometry, as is done in discrete ordinates methods, a Monte Carlo method determines the flux through a stochastic simulation of particle transport. This affords Monte Carlo the ability to find solutions to systems with very complex geometries and with continuous parameters where sufficient discretization is difficult to achieve.

The foundations of Monte Carlo were laid down in the 1940's by Stanisław Ulam (Figure 4) and validated during the Manhattan Project. The simulation consists of modeling a finite number of particles as they evolve through a problem geometry. These particle "histories" then form the basis for determining the flux. Beginning at a source point a particle is "born" or created within the simulation with some initial numerical weight, and an energy and direction chosen at random from a user-defined



Figure 4: Stanisław Ulam

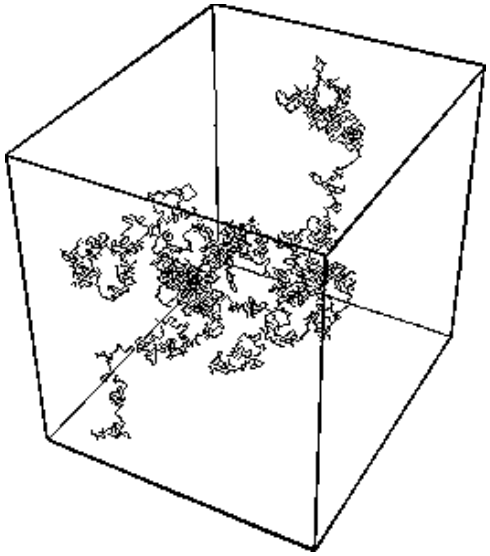


Figure 5: The Random Walk

probability distribution. The random numbers used to select these values are pseudo random numbers based on computer generated numbers uniformly distributed between 0 and 1. The particles are then tracked within the geometry where they interact with the problem's defined materials.

The type of interaction is determined stochastically and is governed by sampling the material region's cross-sectional data. If the particle is absorbed the particle history ends. If, on the other hand, the particle scatters, a new direction is selected at random from the experimentally-determined angular distribution and the resulting energy is calculated from conservation of energy and linear momentum. The particle is then free to travel until it interacts again, at which time the previous process is repeated. This continues until the particle is absorbed or escapes the system. This is known as an *Analog Random Walk* and is illustrated in Figure 5.

If the purpose of the simulation is to determine some quantity in a given region of interest, a tally is maintained for that region that averages each individual particle's contribution to that quantity. Over successive histories a mean value of that quantity is found integrated over some increment of the phase space $\Delta\vec{r}\Delta\hat{\Omega}\Delta E$. As an example, for flux in a region each particle history n will yield some estimate of the flux (defined as the total particle track length in the cell divided by the cell volume),

say ψ_n. This then is the individual particle's contribution to the flux tally integrated over the region, (and possibly if the user desires, over a subset of directions and energies). The average flux over *N* histories becomes:

$$\psi \approx \frac{1}{N}\sum_{n=1}^{N}\psi_n \tag{15}$$

Typically this flux is calculated from the particle's total track length per volume within the region of interest multiplied by its weight. Thus long track lengths from many particles with large weights (corresponding to higher numbers of surviving initial particles) will yield higher fluxes.

From probability theory it can be shown that the statistical error of a tabulated mean quantity within a Monte Carlo simulation decreases with the number of histories asymptotically as $1/\sqrt{N}$. Thus one can calculate to arbitrary accuracy the average value of the flux over a region given a sufficiently large number of histories. In practice however, due to the finite nature of computing resources, very high accuracy may be difficult to achieve economically.

The value of the flux over the entire problem is found by subdividing the geometry into regions and maintaining flux tallies for each region. This can be viewed as setting up a range of "perfect" flux detectors within the geometry. The fineness of spatial detail of the resulting flux map is thus dependant upon the size of the constituent regions, e.g. the number of detectors. This can pose a problem for Monte Carlo; as the number of tally regions increase, the corresponding individual regional volumes decrease and thus the number *N* of particles that enter each region decreases. This then increases the standard deviation and hence the precision of the calculation. Monte Carlo is thus ill-suited to large problems where detailed knowledge of the flux profile is desired. This shortcoming is partially overcome however by Monte Carlo's ability to solve for the flux for virtually any conceivable geometry.

Monte Carlo in Adjoint

Although a Monte Carlo simulation is time-independent, we can intuitively think of physical particles traveling forward in time, from the source to the detector, as they interact with their environment, generating a flux $\psi\left(\vec{r},\hat{\Omega},E\right)$. To utilize Monte Carlo in finding a solution for the adjoint flux $\psi^{\dagger}\left(\vec{r},\hat{\Omega},E\right)$ however, the calculation must be run in "reverse". Thus simulated particles in this case, commonly called *adjunctons*, are born and travel "backwards" through the geometry, from the detector to the source. This process is less physically intuitive than the forward case but is just as valid theoretically.

The adjuncton begins at a defined detector position with some weight and a randomly sampled direction and energy. It then proceeds as before until it interacts, whereby the adjuncton is either absorbed (and the history ends) or it scatters and a new direction and energy is sampled. The key difference is that the scattering distributions are inverted in the adjoint simulation yielding an up-scatter in the adjuncton's energy (with a special normalization weight correction). The adjuncton carries on in this manner until it is terminated as before. The simulation then proceeds with this adjoint treatment of collisions for a finite number of particle histories. For an adjuncton contributing an adjoint flux $\psi^{\dagger}{}_{n}$ with each history to some tally region, the average adjoint flux integrated over the phase space $\Delta\vec{r}\Delta\hat{\Omega}\Delta E$ is given as;

$$\psi^{\dagger} = \frac{1}{N}\sum_{n=1}^{N}\psi^{\dagger}{}_{n} \tag{16}$$

As in the forward case the adjoint flux is determined from the adjuncton's total track length in that region weighted by its adjoint weight and dividing by the region volume. The adjoint tally can likewise conceptually be thought of as an adjuncton detector with the adjoint flux map detail dependant on size of the tally region, i.e. total number of adjoint detectors. And as before in the forward case, the accuracy of the adjoint flux tally is dependant on the number of adjuncton histories run and scales as $1/\sqrt{N}$.

In practice when running a Monte Carlo simulation forward, the sources are representative of the real sources dealt within the problem system and the tallies represent the detectors. If the same problem is run in adjoint, these detectors and sources swap roles. It is then important to note that Monte Carlo automatically normalizes any source distributions before sampling them. Thus the inversion of sources and tallies will necessitate a normalization correction if adjoint detector tallies and corresponding adjoint flux maps are to be directly compared with the results of a forward simulation. This normalization is the ratio of the integral of the spatial, angular and energy densities of the source and the integral of the spatial, angular and energy response function and is described in more detail in Chapter III.

CHAPTER III
TECHNIQUES AND CODES

MCNP 5

Written by Los Alamos National Laboratory (LANL), Monte Carlo N- Particle 5 (MCNP5) is a general purpose, continuous-energy, generalized-geometry, time-dependent, coupled neutron/photon/electron Monte Carlo transport code[5]. A problem is defined for MCNP5 through the creation of a text-based *Input File*. Input files specify the geometry, source, and tallies within the problem as well as listing material compositions with requested cross sections and any additional variance reduction methods. For this project, files are used to set up the parameters by which MCNP5 creates the detector sensitivity maps that indicate CAAS coverage.

MCNP5 by default utilizes a 3-D Cartesian coordinate system and requires the user to define the problem geometry in terms of cells bounded by various surfaces combinatorially. Cells are numbered and assigned a material value and density along with a list of bounding surfaces. Ambiguity in the side of each bounding surface is resolved via the *sense* of the bounding surface given by a sign convention. For example a cell with a bounding x=constant plane with cell points having x coordinates less than the constant denote the plane surface number preceded by a (-), indicating negative sense, while cells with x-coordinates greater than the constant would have the bounding plane number preceded by a (+), indicating a positive sense. Surfaces are expressed in terms of the coefficients of the analytic equations that describe them. For example a plane is described via *X*, *Y* and *Z* intercepts and a right angle parallelepiped, keyword RPP, is described by minimum and maximum values of *X*, *Y* and *Z*. This approach is quite similar to that used by other codes such as KENO, MORSE and VIM.[5] In the random walk, the next particle surface crossing location is determined by calculating the intersection of the particle track's trajectory with each bounding surface of the current cell in order to find the minimum positive distance to an intersection. If the distance to the next interaction site is greater than

this minimum distance, then the particle leaves the current cell, so its new cell is determined and transport continues.

Sources in MCNP5 can be defined as neutron, photon, or electron and can be sampled probabilistically from a source spectrum defined by the user. Although only one type of source particle can be defined in a problem, MCNP5 can track all subsequent particles of any type created in the transport. Source particles are born at a point in MCNP5 and to create a volume source this point must be sampled from a volume distribution. In a similar way, the initial energy and direction of the source particle are sampled from user-specified probability distributions. MCNP5 offers several built-in distributions including Gaussian and Maxwellian.

The user provides MCNP5 with the parameters to be calculated through the specification of tallies. MCNP5 supports several tally types including point, surface, cell and mesh tallies. Point tallies are "scored" at each collision of the particle history. Surface tallies are scored when a particle crosses the surface it is associated with. Cell and mesh tallies score when particles cross the cell or the regions in the mesh. Mesh tallies are defined separately from and superimposed on top of the physical geometry of the problem (Figure 6).

In general, when creating a dose or sensitivity map it will be these mesh tallies that are utilized. Cartesian meshes are defined by specifying the limits of the mesh in *X*, *Y* and *Z*, along with the number of divisions in each direction following.

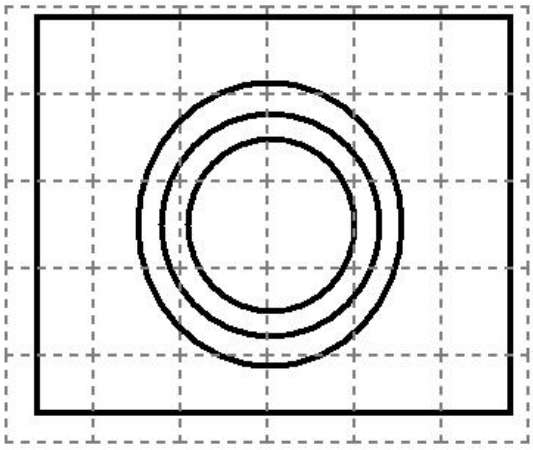


Figure 6: Mesh Grid Tally Superimposed on Annular Geometry

In addition, energy dependence can also be defined. Point tallies are utilized when checking the validity of a forward versus an adjoint calculation for their ease of interchange with point sources. For all tallies, MCNP5 performs ten pass/no-pass statistical checks to help the user determine the quality of the result. This is in addition to tally fluctuation charts which show how a tally's mean, error, variance of the variance, and slope of the largest history scores fluctuate with respect to the number of histories run.

Tallies can be transformed via energy dependant response functions which can be specified by the user in either histogram form or as connected line segments. These functions can redefine a flux tally in many ways including reaction rate, power, and of specific interest here, absorbed dose. It is important to note that MCNP5 does not apply response functions to mesh tallies. Thus mesh tally data has to be further modified by hand via post-processing, which is tedious.

MCNP5 utilizes many sources of nuclear data; these include the Evaluated Nuclear Data File (ENDF) system, the Advanced Computational Technology Initiative (ACTI), the Evaluated Nuclear Data Library (ENDL), Evaluated Photon Data Library (EPDL), the Activation Library (ACTL) from Lawrence Livermore National Laboratory (LLNL), and evaluations from the Nuclear Physics T–16 Group at LANL.[5] These libraries are then processed by codes such as NJOY for use with MCNP5. These cross-section libraries contain reaction information for over 100 elements and isotopes which are identified by atomic number and atomic mass.

MCNP5 also supports a wide variety of variance reduction techniques including Russian roulette, weight windows and particle splitting that may be helpful in some problems where large statistical errors are encountered. How these various techniques are applied and how they affect an adjoint Monte Carlo calculation is beyond the scope of this project.

MCNP 5 in Adjoint

The following methodology for running MCNP5 in adjoint is based on the general guidelines presented in Oak Ridge National Laboratory's *MCNP: Multigroup/Adjoint Capabilities*, by Dr. J. Wagner, et al.[4] While MCNP5 has an

adjoint capability built-in, as of this time it is not capable of running in adjoint with continuous energy cross sections. Rather, adjoint calculations can only be run in a multigroup mode. Monte Carlo has a number of interesting applications in multigroup including comparison of results with deterministic methods and utilization of multigroup cross-sections where continuous ones may be unavailable.

In a multigroup energy representation, the energy domain is covered with a series of contiguous energy regions called groups; cell particles in the same group are assumed to behave alike. The number of groups depends on the number of groups in the available multigroup library. MCNP5 comes with a standard set of multigroup cross sections, MGXSNP, which has 12 photon group and 30 neutron groups (Figure 7) for 99 elements and isotopes. (See Appendix A) If other multigroup cross sections are desired, they can be imported via the CRSRD computer code, which is included when MCNP5 is installed. CRSRD transforms multigroup cross sections into a format usable by MCNP5 utilizing the Carter-Forest treatment. In defining an MCNP5 problem with the multigroup option, the user must supply a source energy spectrum that mimics the group energy structure; all tally energy bin schemes must likewise be translated into the multigroup energy structure.

Photon 12-Group	
Group #	Energy (MeV)
1	20
2	9
3	8
4	7
5	6
6	5
7	4
8	3
9	2
10	1
11	0.5
12	0.1

Neutron 30-Group			
Group #	Energy (MeV)	Group #	Energy (MeV)
1	17.000	16	0.1840
2	15.000	17	0.0676
3	13.500	18	0.0248
4	12.000	19	0.00912
5	10.000	20	0.00335
6	7.790	21	0.001235
7	6.070	22	4.54E-04
8	3.680	23	1.67E-04
9	2.865	24	6.14E-05
10	2.232	25	2.26E-05
11	1.738	26	8.32E-06
12	1.353	27	3.06E-06
13	0.823	28	1.13E-06
14	0.500	29	4.14E-07
15	0.303	30	1.52E-07

Figure 7: MCNP5 MGXSNP Multigroup Structure

It is important to note that the energy dependence (response function) of mesh tallies is not specified like the energy dependence of other tallies, but requires an EMESH parameter. MCNP5 cannot track more then six EMESH tallies for a given FMESH of moderate detail at a time. This necessitates specifying several FMESH's in the problem or breaking a problem up into a series of multiple problems in order to get a mesh tally over an energy range for each group.

MCNP5 cannot plot the results of mesh tallies. Mesh tally data is output by MCNP5 into a separate file MSHTAL, which lists in columnar or matrix format the Cartesian coordinates of each mesh element and its corresponding tally value along with the calculated standard deviations. This data can then be manipulated via post-processing to take into account group-wise response functions and plotted.

Once the problem has been set up in multigroup the conversion to adjoint is not difficult. As described in the theory section, the source and detector must swap places. Thus the source and point tally exchange locations along with their respective source spectrum and detector response histograms. In MCNP5 these are given under the SI and SP keywords which would be interchanged for the values under E and EM respectively. Once the detector and sources have been successfully swapped, a renormalization factor must be introduced to take into account MCNP5's automatic normalization of the source spectrum. This factor – first described in the theory section and expressed as a weight in MCNP5 - can be found by taking the sum of the spatial, angular, time and energy group sources and dividing them by the sum of the spatial, angular, time and energy group responses of the adjoint problem. The source and response are assumed to be universally distributed in space over their respective volumes. Their normalized spatial densities are then simply the inverse of their volumes, or $1/V_s$, for the source, or, $1/V_r$ for a tally region. The normalized angular densities are given by the inverse of the sum of any given angular distributions, or simply $1/4\pi$ in the case of isotropy. Time density is up to the user, and in practice is often given as unity. Next, in the forward problem the energy density normalization is given by each source probability divided by the sum of the source probabilities $P_g / \Sigma P_g$ given under the SP keyword; for the adjoint, it is each response divided by

the sum of the responses $R_g / \Sigma R_g$ listed under EM. Finally the energy responses are given by R_g in the forward problem and the interchanged P_g in the adjoint. These values can be summarized by the table given in Figure 8.[4]

Once the normalization weight is calculated, it can be implemented in one of two ways into the adjoint problem. It can be simply weighted in with the initial importance of the source particles with the WGT keyword defining the source, or it can be added as a global tally multiplier with an FM entry. Fortunately MCNP5 does apply the value of tally multipliers to mesh tallies negating the need to apply the normalization correction in post-processing.

Finally, it is important to remember that in adjoint the particles will up-scatter in energy as they interact, necessitating the addition of a CUT card with some upper bound. It then becomes a matter of the MGOPT keyword with the letter A and the adjoint problem is ready to be run. Once an adjoint problem has been executed successfully the results of any point flux tally can be compared to the corresponding tally in the forward problem for which it was interchanged. Good agreement between these two responses is indicative of the validity of the adjoint computation as outlined in the previous chapter.

In addition to its use in detector sensitivity, Monte Carlo running in adjoint has found a number of other useful applications including cross-section sensitivity studies and charged particle transport.[4]

NORMALIZATION WEIGHT		
	Forward	Adjoint
Spatial Density	$1/V_S$	$1/V_R$
Direction Density	$1/4\pi$	$1/4\pi$
Time Density	1	1
Energy Density	$P_g/\Sigma P_g$	$R_g/\Sigma R_g$
Spatial Response	1	1
Direction Response	1	1
Time Response	1	1
Energy Response	R_g	P_g

Figure 8: Calculation of Normalization Weighting Factor[4]

Data Post-Processing

As mentioned earlier MCNP5 does not apply response functions to mesh tallies and lacks the ability to plot them. To accomplish these two tasks separate codes are needed. Many commercial programs are available that can perform the necessary data handling operations graphically. Outlined here is one methodology utilizing two commercial software packages, Microsoft's Excel® spreadsheet and MicroCal's Origin Pro 7.

Mesh tally output imbedded in the MESHTAL file is normally presented in one of two formats. The first output format is the default without any specified keywords and corresponds to an output consisting of a series of six constant width columns after a series of header lines. To extract this data the entire MESHTAL file is imported into Excel via its input data feature. The first column represents the upper bound of the mesh's energy group which separates out the multiple meshes specified by the EMESH parameter of the FMESH command in the input file. The next three columns indicate the Cartesian coordinates of the mesh boundaries as given by the IMESH, JMESH and KMESH parameters. The fifth column indicates the tally value and the sixth gives an estimate of tally error. The fifth column's values are multiplied by the dose response factor from the response histogram corresponding to its EMESH energy range that was not applied by MCNP5 during the run. Once all of the meshes for each energy group and each type of source particle are gathered together the individual tallies, now doses, can be summed to give one final net dose for each mesh region. This final column is then the final mesh to be plotted. The data can be imported to a second software package Origin Pro 7. Within Origin Pro 7 the columnar data can be expanded into a matrix in a regular way by number per column. This number of rows by columns will correspond to the number of divisions defined in the IMESH, JMESH and KMESH parameters. Once a matrix is generated from the data a contour plot can be created.

The second output format involves the use of the OUTPUT = IJ keyword and parameter. This is the more convenient format as the output is presented already in matrix form with a series of matrices representing the mesh geometry with the tally

value and error. These matrices can be directly imported into Excel and plotted or as in this project sent to Origin Pro 7.

Once the plots are created the scale is adjusted to display contours representing the minimum accident of concern or detector setpoint. The former will serve as a validation check and the latter will determine areas of sufficient CAAS coverage. These plots can then be overlayed with any geometrical information or labels as necessary.

CHAPTER IV
BENCHMARKING AND VALIDATION

The Benchmark Example

To validate this methodology of establishing CAAS coverage, a detector sensitivity map from a benchmark adjoint MCNP5 calculation is compared to the empirical results of Sandia testing and to an analytical approximation as outlined in ANS/ANSI 8.3, Appendix B. The benchmark example is a simple air-ground interface extending 1000 by 1000 meters. Centered within is a point detector located 2 meters above the ground and an accident source 2 meters away at the same elevation. An 84 x 84 mesh grid tally extends laterally throughout the geometry and rises from 1.5 to 2.5 meters above ground level (Figure 9).

The air is a standard atmosphere composed of 79% nitrogen and 21% oxygen in atom % with a density of 1.22 x 10^{-3} g/cm^3. The ground is an earth composition of 16% hydrogen, 57% oxygen, 8% aluminum and 19% silicon in atom % and with a density of 1.70 g/cm^3. These compositions are standard ones outlined in ANS/National Standard 6.6.1.

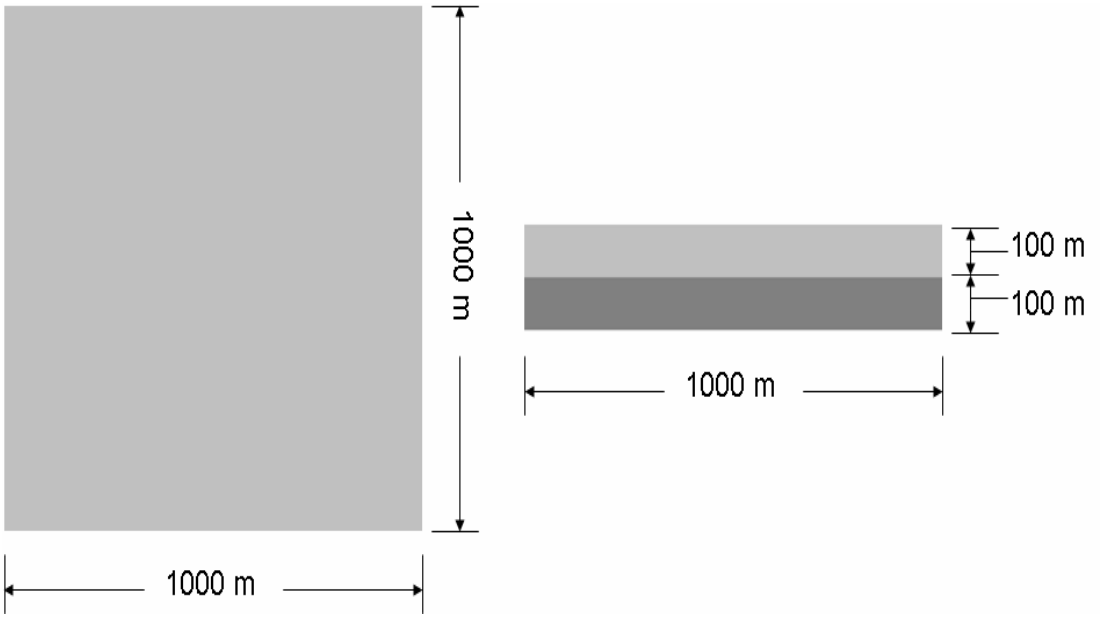


Figure 9: Benchmark Example Geometry

Source Spectra

The source spectra used in this benchmark problem describes bare uranium metal criticality leakage at a density of 18.9 kgU/liter. In these spectra the photons have 39 energy groups and the neutrons have an 18 energy group structure, which is incompatible with the 12 and 30 group structures of the given MGXSNP multigroup library. These spectra must be converted to the necessary number of groups before they can be used. To convert these source spectra, two separate MCNP5 runs are created where these two spectra are tied to a photon or a neutron point source in a vacuum and surrounded by a spherical surface tally. The tally in turn has an energy bin structure that mimics the desired 12 and 30 groups. The resulting tally values from the Monte Carlo simulation give the source spectrum in the needed energy groups with the values representing the initial energy probabilities. Since MCNP5 automatically normalizes the distribution before it samples, no further manipulation of these values is needed and they can be immediately used to form the source spectrum. The input file for accomplishing this conversion is given in Appendix B along with the result.

Dose Rate Response Function

To determine the absorbed dose rate from the source all tallies have a dose response function applied. The utilized function is the International Commission on Radiation Units (ICRU) – 44 Kerma factors for air. Like the source histogram the dose response function must be converted into a form we can use. Being a distribution, in this case it must be piece-wise integrated to yield a histogram. The integrations are conducted over a range of energies that will again correspond to the 12 and 30 group structure of the given MCNP5 multigroup cross-section library. The resulting histogram contains the factors needed to convert a flux tally into an absorbed dose rate in rad/s.

Source Strength Calculation

Before an accurate benchmark can be run a source strength corresponding to the minimum accident of concern of 0.333 rad/s at 2 meters must be determined. Two

initial calculations, one of neutrons, another with photons, with the above geometry and source and response histograms were run with a WGT parameter of unity. The resulting doses at 2 meters given by MCNP5 for neutrons and photons respectively are summarized from the output files in Figure 10:

Based on ANS 8.3, Appendix B, a ratio of neutrons to gamma rays of 2.7 was chosen in reference to an unmoderated assembly. Utilizing this value, a simple algebraic equation is set up with the sum of the product of 2.7 times the neutron dose plus the photon dose all multiplied by some unknown WGT and then set equal to 0.333 rad/s:

$$\left(2.7 \cdot 8.8721 \times 10^{-2} + 9.3173 \times 10^{-2}\right) \cdot WGT = 0.3333 \qquad (19)$$

Solving for the above relation yields a necessary WGT parameter of 9.64419 x 10^{13}.

Benchmark Results

The benchmark calculation as described above was first run in the forward regime for both neutrons and photons. This yielded a dose at the detector for neutrons and photons respectively given in Figure 11 as stated in the output files. When the sum is taken for 2.7 times the neutron dose with the photon dose the requisite 0.333 rad/s is returned. The mesh tallies further yielded the following net dose map with a surface contour corresponding to 0.333 rad/s (Figure 12). The contour reveals a circle of radius 2 meters and is indicative of a source providing a dose of 0.333 rad/s at 2 meters which correctly defines the necessary source term for the ANS 8.3 minimum accident of concern.

The benchmark problem was then run in multigroup adjoint with modifications made as per Chapter III to the input file, e.g. the source term and detector term switch parameters; the source and response histograms interchange; application of a normalization correction, etc. The resulting dose at the adjoint detector (the source location in the forward problem) is given in Figure 13.

7168000	9.1958E-16	0.0008	0.0037	1.4	24696	7168000	9.6624E-16	0.0004	0.0719	2.4	461550
7680000	9.1992E-16	0.0008	0.0148	1.3	22050	7680000	9.6614E-16	0.0004	0.0660	2.4	472599
8192000	9.1999E-16	0.0008	0.0133	1.4	22319	8192000	9.6621E-16	0.0004	0.0618	2.4	488009
8704000	9.2072E-16	0.0010	0.1990	1.4	12563	8704000	9.6627E-16	0.0004	0.0558	2.5	490670
9216000	9.2047E-16	0.0010	0.1888	1.4	12951	9216000	9.6616E-16	0.0004	0.0521	2.4	501445
9728000	9.2020E-16	0.0010	0.1792	1.4	13313	9728000	9.6616E-16	0.0004	0.0479	2.4	505507
10000000	9.1994E-16	0.0009	0.1746	1.4	13500	10000000	9.6610E-16	0.0003	0.0466	2.4	512236

Figure 10: Source Strength Calculation of Neutrons and Photons with WGT=1

7168000	8.8686E-02	0.0008	0.0037	1.4	24684	7168000	9.3186E-02	0.0004	0.0719	2.4	460137
7680000	8.8719E-02	0.0008	0.0148	1.3	22060	7680000	9.3176E-02	0.0004	0.0660	2.4	471211
8192000	8.8725E-02	0.0008	0.0133	1.4	22332	8192000	9.3184E-02	0.0004	0.0618	2.4	486554
8704000	8.8796E-02	0.0010	0.1990	1.4	12569	8704000	9.3189E-02	0.0004	0.0558	2.5	489225
9216000	8.8772E-02	0.0010	0.1888	1.4	12956	9216000	9.3179E-02	0.0004	0.0521	2.4	500027
9728000	8.8746E-02	0.0010	0.1792	1.4	13317	9728000	9.3178E-02	0.0004	0.0479	2.4	504062
10000000	8.8721E-02	0.0009	0.1746	1.4	13503	10000000	9.3173E-02	0.0003	0.0466	2.4	510796

Figure 11: Benchmark Forward Calculation, Neutrons and Photons

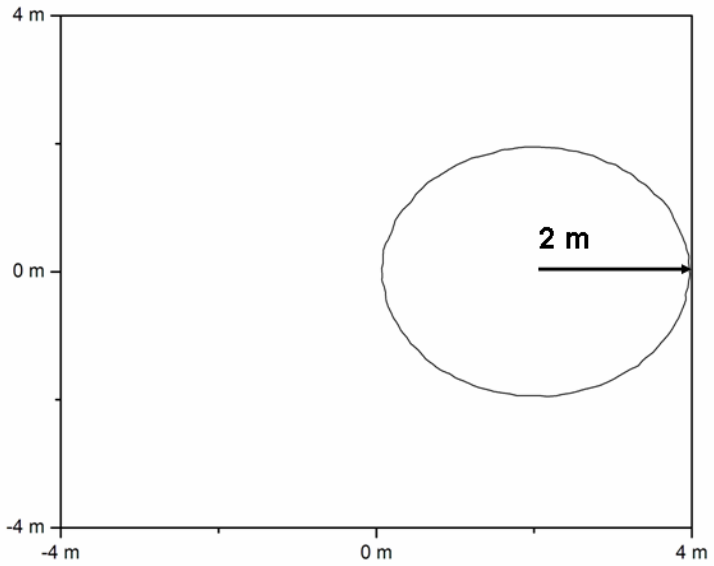


Figure 12: Benchmark Forward Dose Map (0.333 rad/s contour)

655360000	8.8720E-02	0.0004	0.2625	2.3	23650	655360000	9.3285E-02	0.0003	0.4901	2.4	41665
720896000	8.8713E-02	0.0003	0.2527	2.4	25508	720896000	9.3283E-02	0.0003	0.4604	2.3	44504
786432000	8.8709E-02	0.0003	0.2428	2.4	27231	786432000	9.3280E-02	0.0003	0.4321	2.2	47098
851968000	8.8707E-02	0.0003	0.2337	2.4	28866	851968000	9.3277E-02	0.0003	0.4135	2.2	49980
917504000	8.8703E-02	0.0003	0.2263	2.5	30499	917504000	9.3271E-02	0.0002	0.3952	2.1	52667
983040000	8.8700E-02	0.0003	0.2182	2.4	32003	983040000	9.3268E-02	0.0002	0.3840	2.2	55687
1000000000	8.8698E-02	0.0003	0.2163	2.4	32384	1000000000	9.3267E-02	0.0002	0.3810	2.2	56439

Figure 13: Benchmark Adjoint Calculation, Neutrons and Photons

A comparison of the forward and adjoint doses indicate a difference of 2.3 x 10^{-5} rad/s for neutrons and 9.4 x 10^{-5} rad/s for photons, or approximately 0.03% and 0.1% respectively. It can be reasonably concluded that this confirms the result of Chapter II, whereby the adjoint response at the forward source location is equivalent to the forward response at the adjoint source location. Theoretically this demonstrates the legitimacy of the adjoint calculation with respect to the forward benchmark. The mesh tallies further reveal the following detector sensitivity map (adjoint dose map) with a 0.333 rad/s contour plotted (Figure 14):

The contour appears to represent a circle of radius 2 meters and strongly correlates with the results of the forward calculation. This further demonstrates the legitimacy of the calculation as this identical contour (albeit translationally shifted by 2 meters due to source location) is generated from the adjoint source spectrum and adjoint response function.

Validation

To validate the benchmark calculation the results are compared against Sandia testing and ANS 8.3. The above adjoint dose map (detector sensitivity map) is re-scaled to indicate a 1.3889 x 10^{-9} rad/s (0.0005 Gy/hr) contour (Figure 15) which corresponds to the detector setpoint given in Sandia's testing.[2]

The contour presented in the detector sensitivity map in Figure 15 corresponds to an average radius of detectability of the minimum accident of concern of 259 m. The benchmark calculation result is approximately twice the 400' (122 m) radius found by Sandia empirical testing with nominal shielding.[2] This implies that a conservative estimate of a final detectability contour would be roughly half as deep in radius as that indicated through adjoint Monte Carlo calculations if those calculations are compared solely to Sandia's empirical results.

ANS 8.3, Appendix B states that for an unmoderated rapid transient source, which corresponds to the utilized benchmark source spectrum, the following equation can be used to find the radius of coverage analytically;

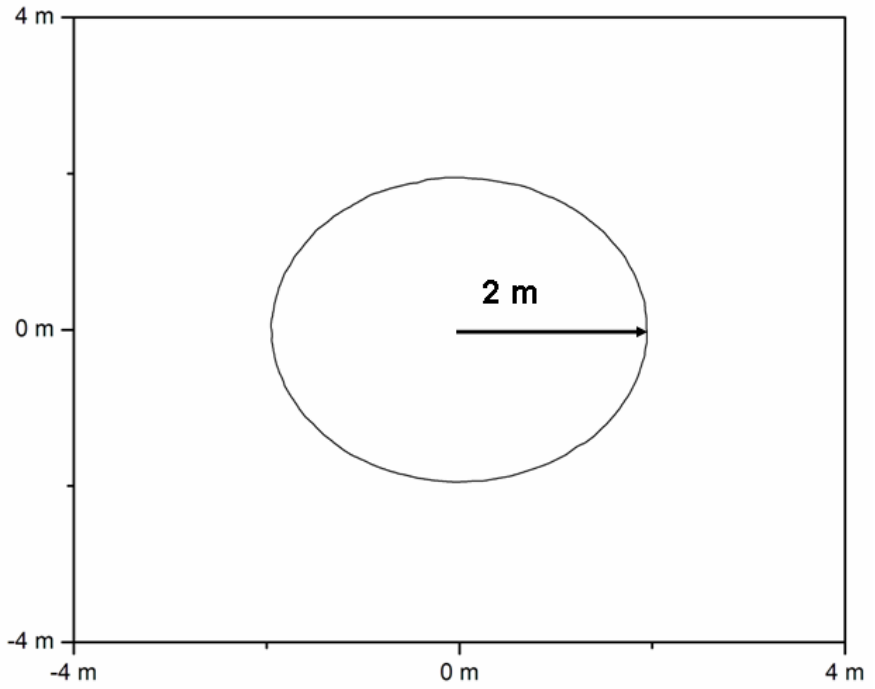


Figure 14: Benchmark Adjoint Dose Map (0.333 rad/s contour)

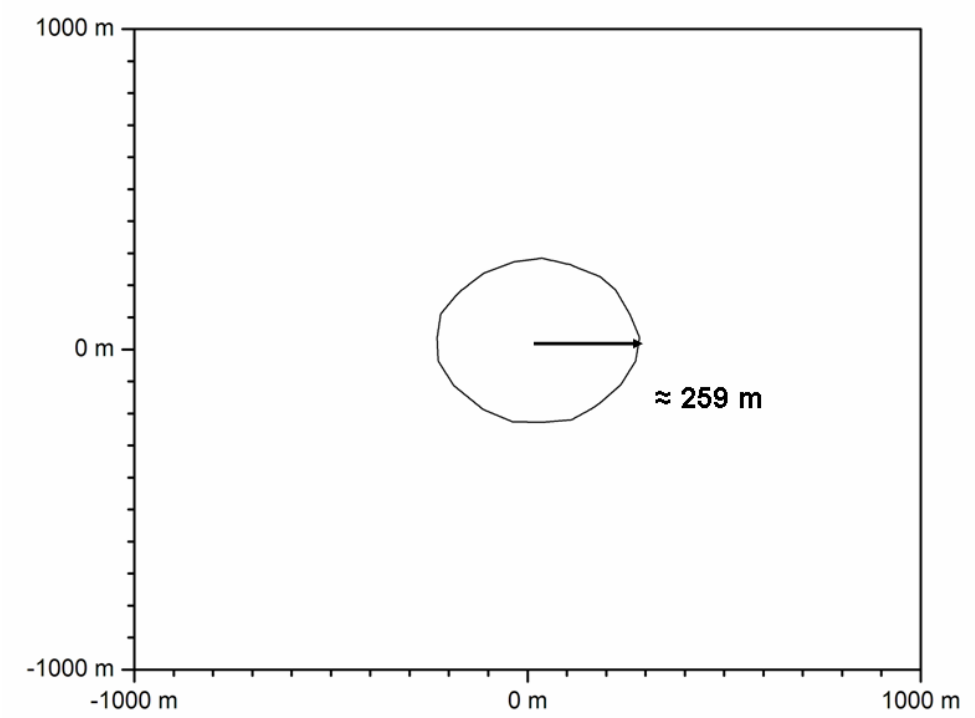


Figure 15: Bench Detector Sensitivity Map, 1.4 x 10^{-9} rad/s (0.0005 Gy/hr) Contour

$$D_r(r) = D_{2m} \times \left(\frac{2}{r}\right)^2 \times t_{air} \times \varepsilon \tag{20}$$

Where $D_r(r)$, the dose rate at r meters and D_{2m} is the dose rate at 2 meters, t_{air} is the transmission factor for air and ε is the assumed detector response to a fast transient. Utilizing the minimum accident of concern of 0.333 rad/s for D_{2m}, 1.3889 x 10^{-9} rad/s for $D_r(r)$, 1/3 for t_{air} and 1/2500 ε all as per ANS 8.3 then solving for *r* yields the following radius of coverage;

$$r = 2 \cdot \sqrt{\frac{D_{2m} \cdot t_{air} \cdot \varepsilon}{D_r(2m)}} \sim 2 \cdot \sqrt{\frac{(0.333)(1/3)(1/2500)}{1.3889 \times 10^{-9}}} \approx 357.59\,m \tag{21}$$

This value for the radius of detectability is nearly a full 100 m larger then that found in the benchmark calculation and represents a 38 % increase. Thus one can assume that any contour found through adjoint Monte Carlo calculations is conservative by around a third on the basis of ANS 8.3's analytical result alone.

Taken all together the adjoint Monte Carlo detector sensitivity mappings yield a benchmark contour with a radius that represents roughly an average between empirical results from Sandia and the analytical approximation of ANS 8.3, Appendix B (Figure 16).

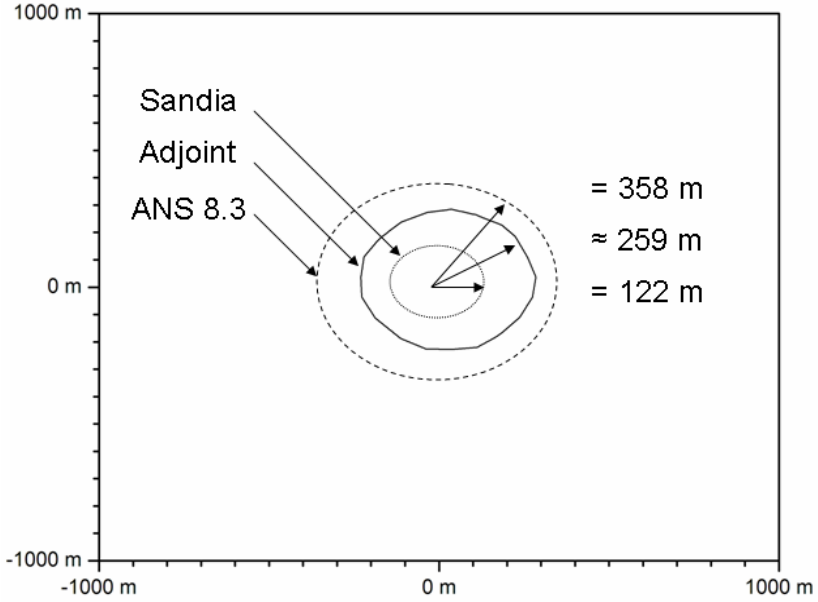


Figure 16: Adjoint Calculation vs. Sandia Empirical vs. ANS 8.3 Analytical Approx.

The adjoint detector sensitivity maps should be considered valid if the above relations are noted and adjusted for when producing final contours corresponding to areas of sufficient coverage, depending on which external result, the empirical or analytical is considered more valid. Since the actual contour produced by MCNP5 adjoint represents a rough average of the two, it will be utilized here as the final contour for determining zones of adequate CAAS coverage. With this result the novel methodology will, for the remainder of this work, be considered validated.

CHAPTER V
CONCEPTUAL STORAGE FACILITY EXAMPLE PROBLEM

The Example Storage Facility

To demonstrate the adjoint method for establishing CAAS coverage, a conceptual building with 110,025 ft^2 of floor space was studied with MCNP5 (Figure 17). This generalized model consists of an empty concrete shell with 4 feet thick concrete walls and ceiling and a 10 ft foundation. The concrete is composed of 10% hydrogen, 58% oxygen, 1.4% sodium, 0.2% magnesium, 3.2% aluminum, 21% silicon, 1% potassium, 3.9% calcium and 0.4% iron in atom percent and with a density of 2.34 g/cm^3, which is the same composition found in the ANS National Standard 6.6.1. With walls 105' by 105' (interior) the ceiling stands at a height of 40 feet. Surrounding the shell above ground level and inside is standard atmosphere with the same composition used in the benchmark example. Below ground level and surrounding the foundation is likewise simulated earth with a composition taken previously. The outer boundaries of the problem extend to 100' laterally and from 20 feet below the surface to 50 feet into the air vertically from the surface.

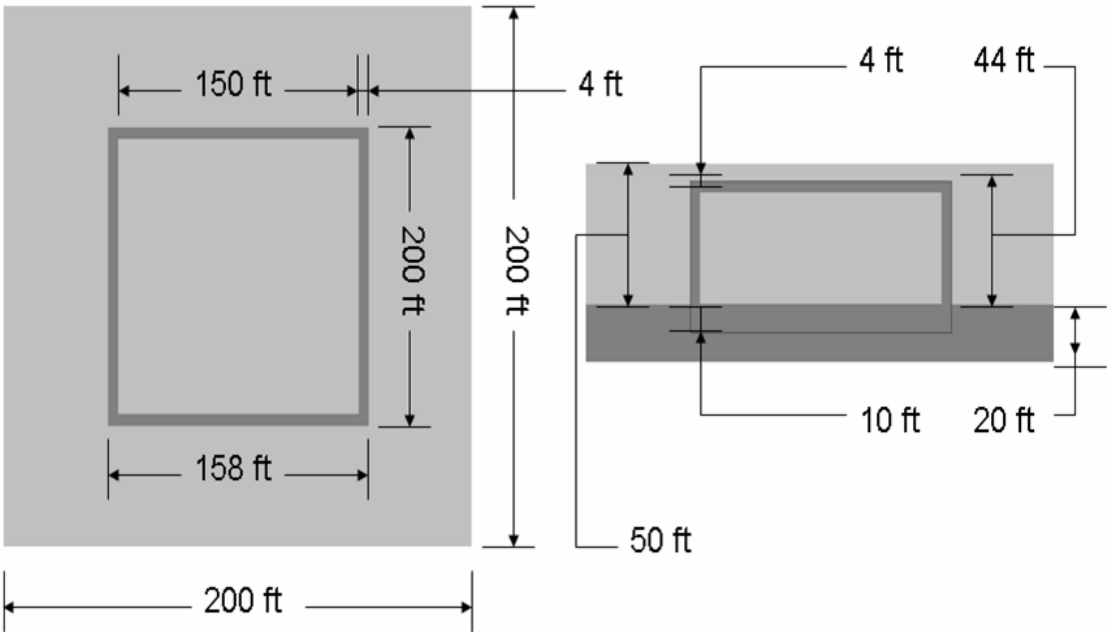


Figure 17: Example Storage Facility

RCSB Configuration

To simulate the effects of neutron absorbing materials in the vicinity of CAAS detectors and to measure their impact on detector coverage, added to the model building's interior are a number of model Rackable Can Storage Boxes (RCSB's) based on the configuration given in Figure 18. The RCSB has been proposed as a storage medium for highly enriched fissile materials and may be present in areas where a criticality accident with a spectrum similar to the benchmark example may be of concern. The RCSB is composed mostly of Eagle Picher Technologies' BoroBond4^{TM}. BoroBond has a density of 1.91 g/cm^3 and is a 4.10 weight percent B_4C borated, chemically-bonded, phosphate-based ceramic solid formed from the exothermic reaction[3];

$$MgO(powder) + KH_2PO_4(powder) + 5H_2O(liquid) \rightarrow MgKPO_4 \cdot 6H_2O(solid) \quad (19)$$

The RCSB's are designed to store up to six cylindrical slugs of up to 20 kg of highly enriched uranium (HEU) material in six drilled out holes 10 inches apart. The boron content of the BoroBond helps prevent criticality but at the same time may act as an effective shield against accident particle transport to a CAAS detector. For the

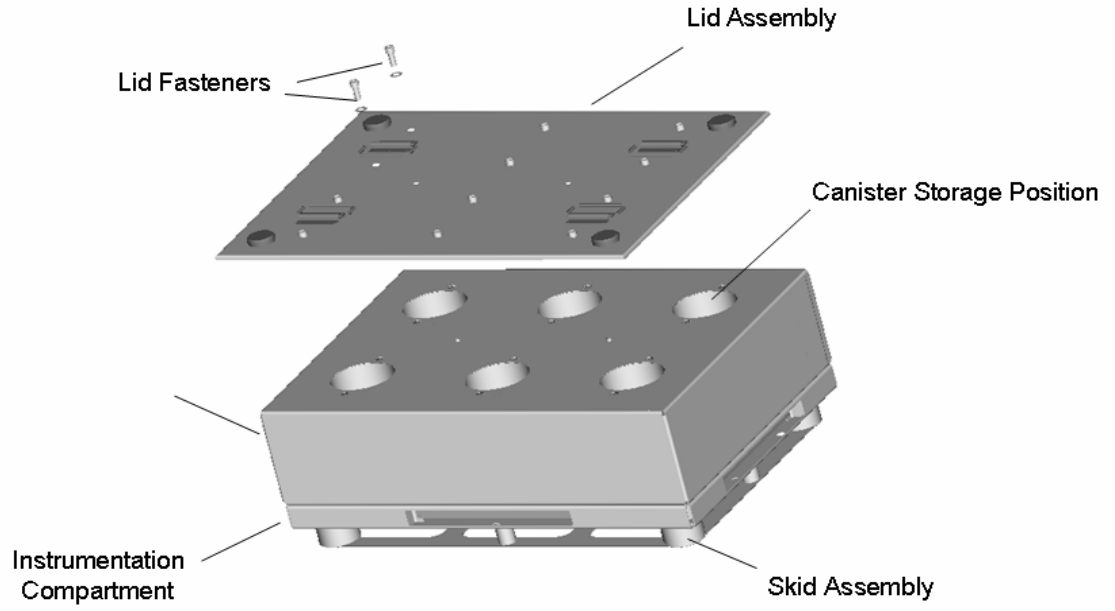


Figure 18: The Rackable Can Storage Box

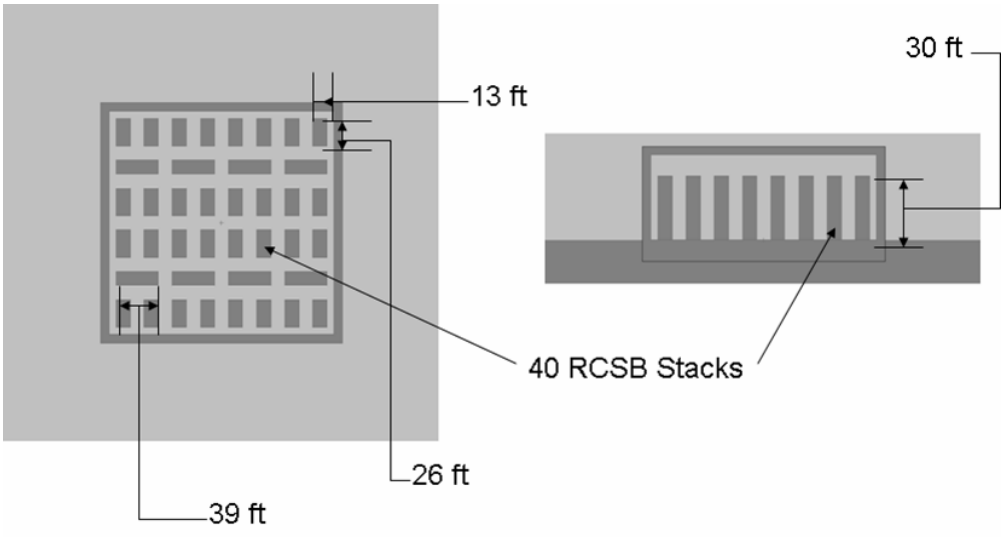


Figure 19: Example Storage Facility w/ 40 RCSB's

purposes of modeling, the HEU material will be ignored and the RCSB will be presented as a large stack, homogenized into a single slab 13' by 26' by 30' tall. In total 42 of these stacks and eight 39' long ones are added to the geometry with representative corridor spacing between to yield the final conceptual model given in Figure 19.

Example Problem Setup

The example problem utilizes the same uranium metal leakage source spectrum as the benchmark problem and is located at the center of the facility two meters off the ground. A large 84 x 84 x 1 mesh tally is superimposed on top of this geometry, from 1 to 3 meters above the floor and likewise tied to the same ICRU-44 dose response function as the benchmark problem. In addition to the mesh tally, a point tally with a five mean free path radius of exclusion is placed in the facility directly above the source near the ceiling. This will serve as the source in the adjoint calculation, as well as being a validation check.

Example Problem Results

First run in the forward case the resultant dose map is shown in Figure 20. The plot indicates the highest dose rates right near the source and along the corridors with

clear line-of-sight to it. A detector placed in this general vicinity should conceivably have the largest coverage area. Areas that have RCSB obstruction between them receive far smaller doses with the fewest particles transported to the corners of the geometry. For the highest probability of achieving full CAAS coverage of this conceptual facility, detectors may have to be placed in those corner locations. The total doses received at the point detector on the ceiling from neutrons and photons are shown from the output in Figure 21. Taking 2.7 times the neutron dose rate and adding the photon dose rate yields a total dose rate of 0.019864 rad/s. It is important to note that no dose of consequence was measured outside of the facility walls, thus suggesting that CAAS detectors located inside would have difficulty establishing coverage outside the facility.

With the forward calculation in hand three locations for detector placement (adjoint source) are chosen; at the location of the initial forward detector at the center of the geometry near the ceiling and at the upper right and lower right corners of the geometry, also near the ceiling.

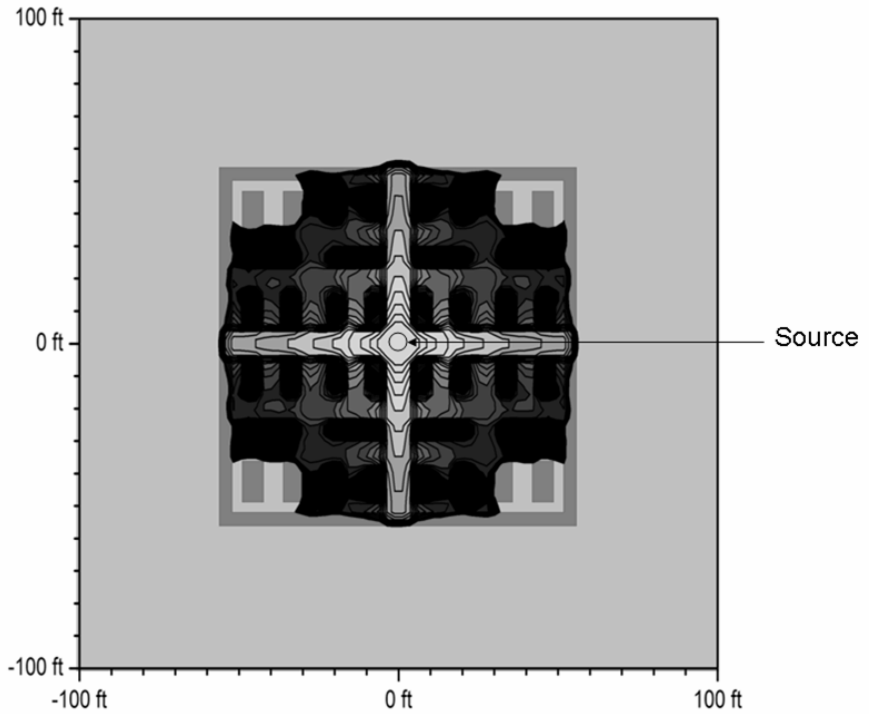
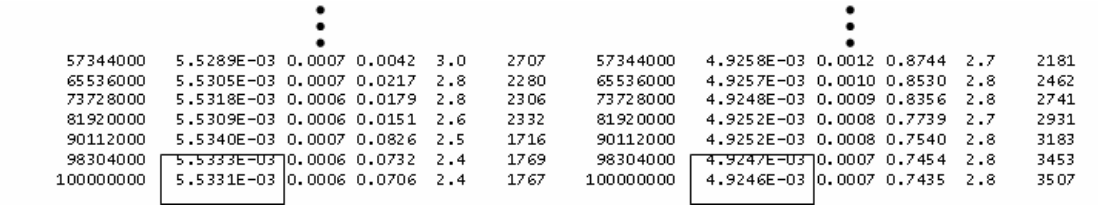


Figure 20: Example Storage Facility Dose Rate Map



57344000	5.5289E-03	0.0007	0.0042	3.0	2707	57344000	4.9258E-03	0.0012	0.8744	2.7	2181
65536000	5.5305E-03	0.0007	0.0217	2.8	2280	65536000	4.9257E-03	0.0010	0.8530	2.8	2462
73728000	5.5318E-03	0.0006	0.0179	2.8	2306	73728000	4.9248E-03	0.0009	0.8356	2.8	2741
81920000	5.5309E-03	0.0006	0.0151	2.6	2332	81920000	4.9252E-03	0.0008	0.7739	2.7	2931
90112000	5.5340E-03	0.0007	0.0826	2.5	1716	90112000	4.9252E-03	0.0008	0.7540	2.8	3183
98304000	5.5333E-03	0.0006	0.0732	2.4	1769	98304000	4.9247E-03	0.0007	0.7454	2.8	3453
100000000	5.5331E-03	0.0006	0.0706	2.4	1767	100000000	4.9246E-03	0.0007	0.7435	2.8	3507

Figure 21: Example Storage Facility Forward Calculation, Neutrons and Photons

The conversion of the forward example is made to adjoint via the novel methodology outlined in Chapter III for each detector and run. For the first adjoint calculation the detector and source have exchanged locations from their original ones in the forward calculation. We can then compare the resultant dose rates directly, with the adjoint results in Figure 22:

Again multiplying the neutron dose rate by 2.7 and adding the photon dose rate yields a total dose rate of 0.019854 rad/s. This is a difference of 9.52 x 10^{-6} rad/s or 0.05%. It is assumed that this represents a common, *R*, response legitimizing the adjoint calculation with respect to the forward run.

For this first example of a centrally located detector the detector sensitivity map is plotted with a contour representing a detector set-point of 1.3889 x 10^{-9} rad/s in Figure 23, again the same as used in Sandia testing. This is superimposed on the example facility geometry with highlighted areas inside the contour indicating areas of detector coverage. The contour indicates that the centrally located detector is sufficient to detect the minimum accident of concern throughout the geometry. If however we plot out in a similar fashion the detector sensitivity map for the upper right corner detector we find in Figure 24. Note that not the entire geometry has coverage. It appears that a source corresponding to the minimum accident of concern would not be detected if it were located in the vicinity of the lower left corner with a detector setpoint of 1.4 x 10^{-9} rad/s. Likewise, in the final case of a lower right detector the detector sensitivity map indicates that a source corresponding to the minimum accident of concern would escape detection if located in the upper right hand corner as indicated in Figure 25:

57344000	5.5369E-03	0.0022	0.3474	2.3	1521	57344000	4.9098E-03	0.0014	0.0052	4.1	4704
65536000	5.5323E-03	0.0020	0.3255	2.4	1679	65536000	4.9055E-03	0.0013	0.0044	4.5	4858
73728000	5.5331E-03	0.0018	0.3017	2.4	1819	73728000	4.9083E-03	0.0012	0.0040	3.9	4790
81920000	5.5372E-03	0.0017	0.2665	2.3	1901	81920000	4.9112E-03	0.0012	0.0036	4.3	4731
90112000	5.5375E-03	0.0015	0.2459	2.4	2008	90112000	4.9096E-03	0.0011	0.0032	4.7	4820
98304000	5.5380E-03	0.0014	0.2272	2.4	2106	98304000	4.9072E-03	0.0011	0.0028	4.8	4883
100000000	5.5365E-03	0.0014	0.2237	2.4	2124	100000000	4.9059E-03	0.0010	0.0028	5.1	4912

Figure 22: Example Storage Facility Adjoint Calculation, Neutrons and Photons

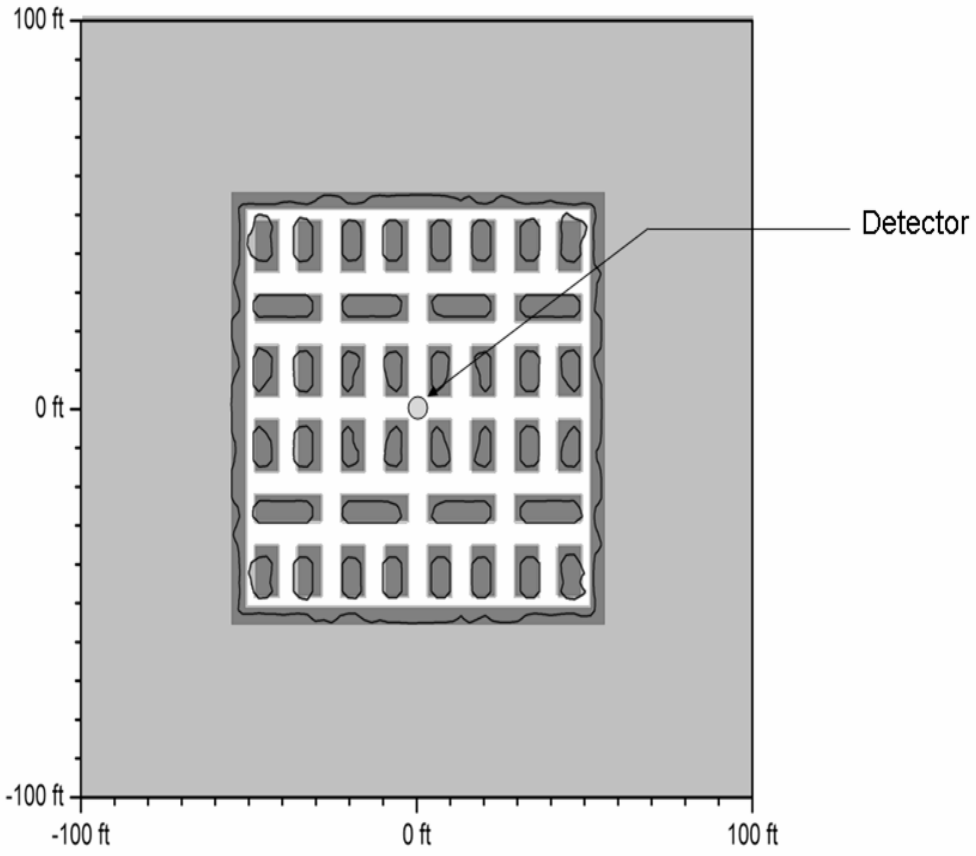


Figure 23: Example Detector 1 Sensitivity Map, 1.4 x 10^{-9} rad/s Contour

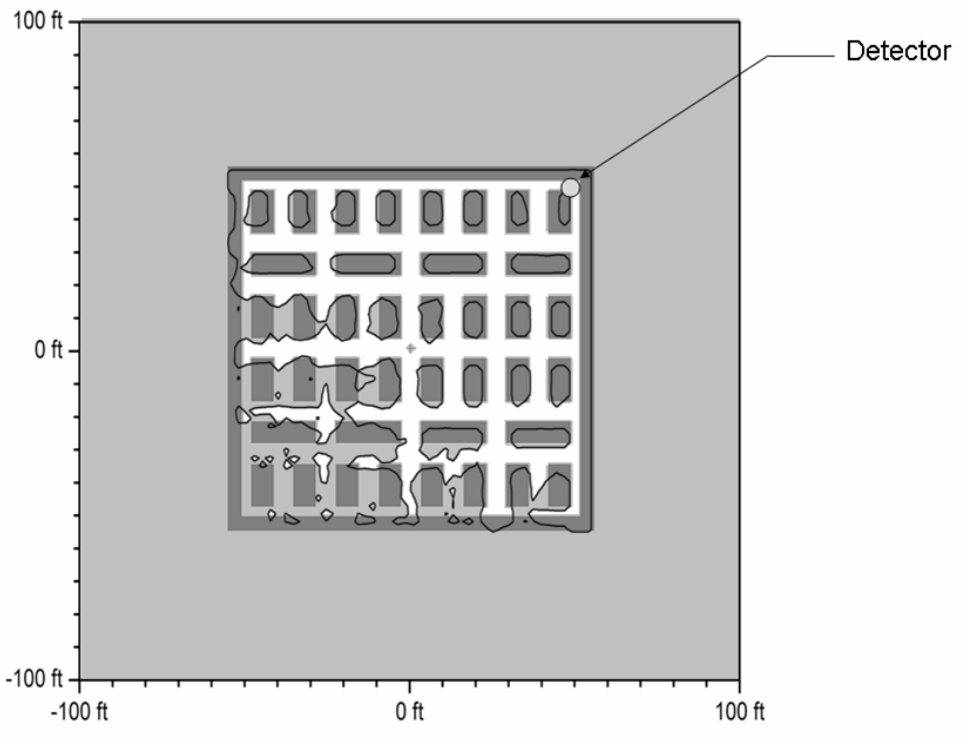


Figure 24: Example Detector 2 Sensitivity Map, 1.4 x 10^{-9} rad/s Contour

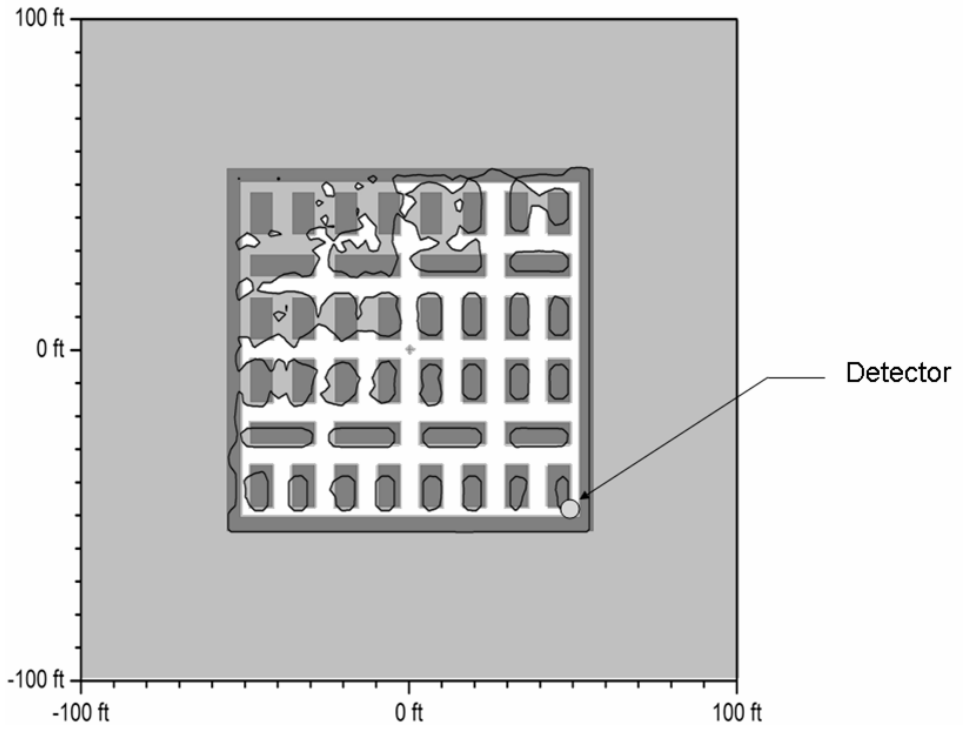


Figure 25: Example Detector 3 Sensitivity Map, 1.4 x 10^{-9} rad/s Contour

From these plots the first thing to notice is the impact line-of-sight plays on detector sensitivity as expected. The more shielding between the detector and possible accident location the more difficult it becomes for a CAAS detector to detect that accident. It is also worthwhile to note that no significant coverage was achieved outside of the concrete facility. This may indicate that CAAS detectors located internally cannot be expected to detect minimum accidents of concern externally of large concrete structures.

CHAPTER VI
MULTIPLE DETECTOR COVERAGE

The redundancy provided by multiple detectors is often a requisite for declaring adequate CAAS detector coverage of an area. The novel methodology for determination of CAAS coverage utilizing MCNP5 in multigroup adjoint as described above can be extended to demonstrate areas of multiple detector coverage as well. This is accomplished by superimposing the detector sensitivity map contours of multiple detectors and highlighting their intersections of coverage. As an example triple-detector coverage is demonstrated in the Chapter V problem by superimposing contours for the three detector locations and highlighting their intersection, which corresponds to all three detectors being able to see the region shown in Figure 26. Thus the highlighted region indicates that a source corresponding to the minimum accident of concern would be detected by no fewer then three separate CAAS detectors, ensuring redundancy.

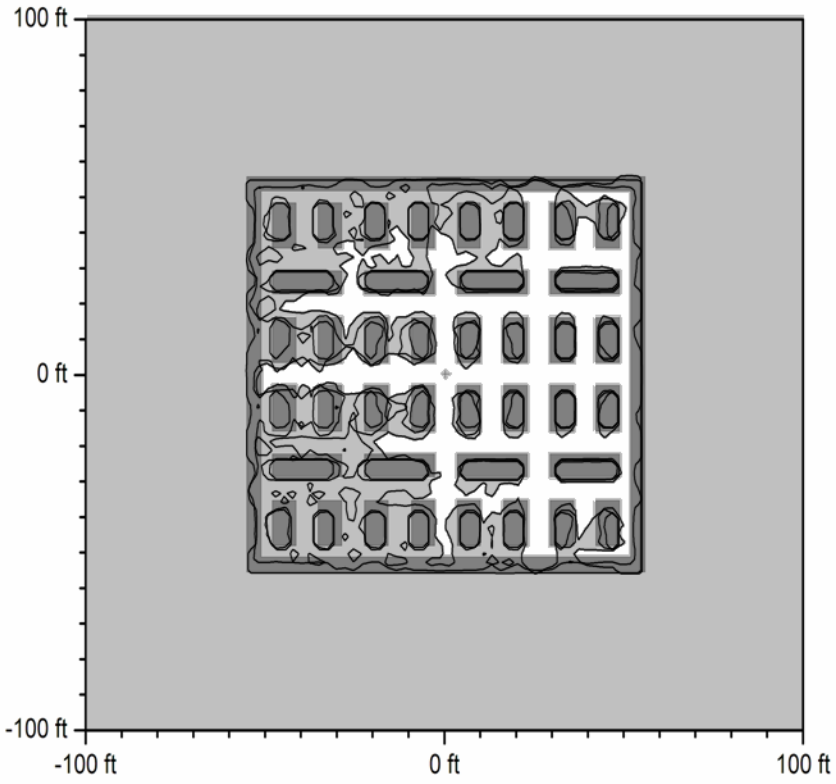


Figure 26: Triple-Detector Coverage Sensitivity Map, 1.4 x 10^{-9} rad/s Contour

CHAPTER VII
CONCLUSIONS AND RECOMMENDATIONS

Supported by a firm theoretical basis, the results of the benchmark and example conceptual storage facility geometry problem demonstrate that Monte Carlo running in adjoint utilizing MCNP5 is capable of generating detector sensitivity maps that can accurately define contours corresponding to regions of adequate detectablity regarding a minimum accident of concern.

The results further indicate the difficulty of transport through dense materials and reinforce line-of-sight in detector placement. Detection through thick concrete was particularly difficult.

This methodology may be rather simply extended to allow definition of full three dimensional detector sensitivity contours. While post-processing and presentation of such data may be difficult the methodology to create it would not be altered significantly.

This methodology must be more thoroughly benchmarked before its use in augmenting the deployment of a live CAAS system. Further work would almost certainly include experimental work comparing actual detector sensitivities with those determined through the adjoint Monte Carlo simulation. In addition the user should keep an eye to applications of newer codes such as MCNPX or updates to MCNP5 that may alleviate some of the data post-processing that is currently necessary.

LIST OF REFERENCES

LIST OF REFERENCES

[1] Image courtesy of the Research Laboratory of Electronics at MIT

[2] Angelo, Peter L., et al. *CAAS Coverage for a New Storage Facility at the Y-12 NSC*, 2005 NSCD Topical Meeting.

[3] Neal, John S., et al. *Gamma Spectroscopy Measurements of BoroBond Blocks*, Oak Ridge National Laboratory, Oak Ridge, TN 37831

[4] Wagner, John C., et al. *MCNP: Multigroup/Adjoint Capabilities* Los Alamos National Laboratory, April 1994

[5] X-5 Team, *MCNP – A General Monte Carlo N-Particle Code Version 5 – Volume 1*. Los Alamos National Laboratory, April 2003

[6] Lewis, E.E., et al. *Computational Methods of Neutron Transport*
© 1993 The American Nuclear Society, Inc.
555 N. Kensington Avenue, Lagrange Park, Il 60525

[7] American Nuclear Society *ANS-8.3 Criticality Accident Alarm System*
© 1997 The American Nuclear Society, Inc.
555 N. Kensington Avenue, Lagrange Park, Il 60525

APPENDICES

APPENDIX A
Table of MCNP 5 Built-In Multigroup Cross Sections

Isotope	ZAID	Source	Isotope	ZAID	Source	Isotope	ZAID	Source
H	1001.50	ENDF/B-V	Ni	28000.50	ENDF/B-V	W	74000.55	Group T-2
D	1002.55	Group T-2	Cu	29000.50	ENDF/B-V	W-182	74182.55	Group T-2
T	1003.50	ENDF/B-V	Ga	3100.50	ENDF/B-V	W-183	74183.55	Group T-2
He-3	2003.50	ENDF/B-V	As-75	33075.35	ENDL85	W-184	74184.55	Group T-2
He-4	2004.50	ENDF/B-V	Kr-78	36078.50	ENDF/B-V	W-186	74186.55	Group T-2
Li-6	3006.50	ENDF/B-V	Kr-80	36080.50	ENDF/B-V	Re-185	75185.50	ENDF/B-V
Li-7	3007.55	Group T-2	Kr-82	36082.50	ENDF/B-V	Re-187	75187.50	ENDF/B-V
Be-7	4007.50	ENDF/B-V	Kr-83	36083.50	ENDF/B-V	Ir	77000.55	Group T-2
Be-9	4009.50	ENDF/B-V	Kr-84	36084.50	ENDF/B-V	Pt	78000.35	ENDL85
B-10	5010.50	ENDF/B-V	Kr-86	36086.50	ENDF/B-V	Au-197	79197.56	Group T-2
B-11	5011.56	Group T-2	Y-98	39089.50	ENDF/B-V	Pb	82000.50	ENDF/B-V
C	6000.50	ENDF/B-V	Zr	40000.50	ENDF/B-V	Bi-209	83209.50	ENDF/B-V
C-12	6012.50	ENDF/B-V	Nb-93	41093.50	ENDF/B-V	Th-232	90232.50	ENDF/B-V
N-14	7014.50	ENDF/B-V	Mo	42000.50	ENDF/B-V	Pa-233	91233.50	ENDF/B-V
N-15	7015.50	Group T-2	Rh-103	45103.50	ENDF/B-V	U-233	92233.50	ENDF/B-V
O-16	8016.50	ENDF/B-V	U-235 FP	45117.90	Group T-2	U-234	92234.50	ENDF/B-V
F-19	9019.50	ENDF/B-V	Pu-239 FP	46119.90	Group T-2	U-235	92235.50	ENDF/B-V
Na-23	11023.50	ENDF/B-V	Ag	47000.55	ENDF/B-V	U-236	92236.50	ENDF/B-V
Mg	12000.50	ENDF/B-V	Ag-107	47107.50	ENDF/B-V	U-237	92237.50	ENDF/B-V
Al-27	13027.50	ENDF/B-V	Ag-109	47109.50	ENDF/B-V	U-238	92238.50	ENDF/B-V
Si	14000.50	ENDF/B-V	Cd	48000.50	ENDF/B-V	U-239	92239.35	ENDL85
P-31	15031.50	ENDF/B-V	Avg. FP	50120.35	ENDL85	Np-237	93237.55	Group T-2
S-32	16032.50	ENDF/B-V	FPP	50998.99	ENDF/B-V	Pu-237	94237.35	ENDL85
Cl	17000.50	ENDF/B-V	FPA	50999.99	ENDF/B-V	Pu-238	94238.50	ENDF/B-V
Ar	18000.35	ENDL85	Xe	54000.35	ENDL85	Pu-239	94239.55	Group T-2
K	19000.50	ENDF/B-V	Ba-138	56138.50	ENDF/B-V	Pu-240	94240.50	ENDF/B-V
Ca	20000.50	ENDF/B-V	Eu	63000.35	ENDL85	Pu-241	94241.50	ENDF/B-V
Ti	22000.50	ENDF/B-V	Eu-151	63151.55	Group T-2	Pu-242	94242.50	ENDF/B-V
V	23000.50	ENDF/B-V	Eu-153	63153.55	Group T-2	Am-141	95241.50	ENDF/B-V
Cr	24000.50	ENDF/B-V	Gd	64000.35	ENDL85	Am-242m	95242.50	ENDF/B-V
Mn-55	25055.50	ENDF/B-V	Ho-165	67165.55	Group T-2	Am-243	95243.50	ENDF/B-V
Fe	26000.55	Group T-2	Tm-169	67169.55	Group T-2	Cm-242	96242.50	ENDF/B-V
Co-59	27059.50	ENDF/B-V	Ta-181	73181.50	ENDF/B-V	Cm-244	96244.50	ENDF/B-V

APPENDIX B
EXAMPLE MULTIGROUP SOURCE DISTRIBUTION CONVERSION INPUT FILES

```
Source Function Conversion to 12-Group
1 0 -7
2 0 1

1 SU 1

MODE P
IMP:P 1 0
SDEF POS = 0 0 0 PART=2 ERG=D1
SI1     0.0001     0.01      0.03      0.05      0.07
        0.1        0.15      0.2       0.25      0.3
        0.35       0.4       0.45      0.5       0.35
        0.6        0.65      0.7       0.8       1
        1.4        1.8       2.2       2.6       2.8
        3.25       3.75      4.25      4.75      5
        5.25       5.75      6.25      6.75      7.5
        9          11        13        15
SP1     0.00000E+00 4.25692E-06 8.81782E-05 4.79981E-05 1.30203E-04
        1.94068E-03 1.03644E-03 4.76115E-04 8.25136E-04 1.24252E-03
        1.98881E-03 2.74196E-03 3.17389E-03 3.75068E-03 6.45291E-03
        4.27073E-03 4.75958E-03 4.88270E-03 9.26523E-03 1.72889E-02
        2.87197E-02 1.96163E-02 1.24909E-02 8.56718E-03 2.78645E-03
        4.46415E-03 2.81418E-03 1.71765E-03 9.05077E-04 2.81315E-04
        2.41787E-04 4.16730E-04 2.19943E-04 9.86855E-05 5.69380E-05
        1.20369E-05 0.00000E+00 0.00000E+00 0.00000E+00
F2:P    1
E0      0.1        0.5       1         2         3
        4          5         6         7         8
        9          20
NPS 1000000
```

```
Source Function Conversion to 30-Group
1 0 -1
2 0 1

1 SO 1

MODE N
IMP:N 1 0
SDEF POS = 0 0 0 PAR=1 ERG=D1
SI1      1.00000E-09 2.50000E-08 1.00000E-07 1.00000E-06 1.00000E-05
         0.0001      0.001       0.01        0.1         0.5
         1           2           2.5         5           7
         10          14          20
SP1      0.00000E 00 0.00000E+00 7.03670E-07 2.72326E-05 3.47370E-04
         1.17726E-03 5.79228E-03 1.81845E-02 4.52106E-02 9.66042E-02
         9.00576E-02 1.09790E-01 3.84695E-02 8.89204E-02 1.74793E-02
         4.94431E-03 6.48550E-04 3.10751E-05
F2:N     1
E0       1.52000E-07 4.14000E-07 1.13000E-06 3.06000E-06 8.32000E-06
         2.26000E-05 6.14000E-05 1.67000E-04 4.54000E-04 1.23503E-03
         3.39000E-03 9.12000E-03 2.48000E-02 6.76000E-02 1.84003E-01
         3.03000E-01 5.00000E-01 8.23000E-01 1.353       1.738
         2.232       2.865       3.880       6.070       7.790
         10          12          13.5        15          20
NPS 1000000
```

APPENDIX C
CONCEPTUAL STORAGE FACILITY EXAMPLE INPUT FILES

```
Empty Model w/ ICRU 44 Response & 16900 gUI Leakage (Photon, Multi Forward)
1 1 -1.70E+0 -1  4
2 2 -1.22E-3 -2  4
3 2 -1.22E-3 -3
4 3 -2.34E+0  3 -4
6 0 1 2

1 RPP -2.288E+03  2.288E+03 -2.288E+03  2.288E+03 -6.096E+02  0.0000000
2 RPP -2.288E+03  2.288E+03 -2.288E+03  2.288E+03  0.0000000  1.624E+03
3 RPP -1.800E+03  1.800E+03 -1.800E+03  1.800E+03  0.0000000  1.219E+03
4 RPP -1.722E+03  1.722E+03 -1.722E+03  1.722E+03 -3.048E+02  1.341E+03

MODE P
IMP:P 1 1 1 1 0
SDEF POS = 0 0 2.000E+02 PART=2 ERG=D1 WGT=1.76181E+14
SI1     0.1       0.5       1         2         3
        4         5         6         7         8
        9         20
SP1       0.00000E-00 8.22642E-03 2.62946E-02 2.93389E-02 1.06373E-02
        3.32394E 03 1.10812E 03 4.17940E 04 1.18909E 04 2.22818E 05
        4.89608E-06 0.00000E+00
FMESH4:P  ORIGIN -1.699E+03 -1.699E+03 1.216E+03
        IMESH 1.699E+3 IINTS 100
        JMESH 1.699E+3 JINTS 100
        KMESH 1.216E+3 KINTS 1
F5:P      2.000E+02 0 2.000E+02 5.0
E0      0.1       0.5       1         2         3
        4         5         6         7         8
        9         20
EM0       7.69900E-12 6.49426E-11 1.73000E-10 6.07600E-10 8.76500E-10
        1.10300E-09 1.31000E-09 1.61000E-09 1.71000E-09 1.91000E-09
        2.11000E-09 3.83060E-09
M1        001000 0.16
        008000 0.67
        013000 0.08
        014000 0.19
M2        UUUUUU U./8UU
        008000 0.2102
M3        001000 0.1049
        008000 0.6843
        011000 0.0140
        012000 0.0019
        013000 0.0319
        014000 0.2108
        019000 0.0092
        020000 0.0389
        026000 0.0041
MGOPT F 12
NPS 100000
```

```
Empty Model w/ ICRU 44 Response & 18900 gUI Leakage (Photon, Multi Adjoint)
1 1 -1.70E+0 -1  4
2 2 -1.22E-3 -2  4
3 2 -1.22E-3 -3
4 3 -2.34E+0  3 -4
6 0 1 2

1 RPP -2.288E+03  2.288E+03 -2.288E+03  2.288E+03 -8.096E+02  0.0000000
2 RPP -2.288E+03  2.288E+03 -2.288E+03  2.288E+03  0.0000000  1.624E+03
3 RPP -1.800E+03  1.800E+03 -1.800E+03  1.800E+03  0.0000000  1.219E+03
4 RPP -1.722E+03  1.722E+03 -1.722E+03  1.722E+03 -3.048E+02  1.341E+03

MODE P
IMP:P 1 1 1 1 0
SDEF POS = 2.000E+02 0 2.000E+02 PART=2 ERG=D1 WGT=1.78181E+14
SI1      0.1        0.5        1          2          3
         4          6          6          7          8
         9          20
SP1      0.00000000 6.49426E-11 1.73000E-10 6.07600E-10 8.76500E-10
         1.10300E-09 1.31000E-09 1.61000E-09 1.71000E-09 1.91000E-09
         2.11000E-09 3.63050E-09
FMESH4:P  ORIGIN -1.699E+03 -1.699E+03 1.999E+02
         IMESH 1.699E+3 INTS 100
         JMESH 1.699E+3 JINTS 100
         KMESH 2.001E+2 KINTS 1
         EMESH 20
F6:P     0 0 2.000E+02 6.0
E0       0.1        0.5        1          2          3
         4          6          6          7          8
         9          20
EM0      1.16729E-03 8.22542E-03 2.52948E-02 2.93369E-02 1.06373E-02
         3.32394E-03 1.10612E-03 4.17940E-04 1.16809E-04 2.22818E-05
         4.89608E-06 0.000000000
FM6      1.91463E-07
M1       001000 0.16
         008000 0.57
         013000 0.09
         014000 0.19
M2       007000 0.7898
         008000 0.2102
M3       001000 0.1049
         008000 0.5843
         011000 0.0140
         012000 0.0019
         013000 0.0319
         014000 0.2106
         019000 0.0092
         020000 0.0389
         026000 0.0041
MGOPT A 12
CUT:P J 20
NPS 100000
```

```
Empty Model w/ ICRU 44 Response & 10000 g/cc Leakage (Neutron, Multi Forward)
1 1 -1.70E+0 -1  4
2 2 -1.22E-3 -2  4
3 2 -1.22E-3 -3
4 3 -2.36E+0  3 -4
5 0 1 2

1 RPP -2.286E+03  2.286E+03 -2.286E+03  2.286E+03 -6.096E+02  0.0000000
2 RPP -2.286E+03  2.286E+03 -2.286E+03  2.286E+03  0.0000000  1.524E+03
3 RPP -1.800E+03  1.800E+03 -1.800E+03  1.800E+03  0.0000000  1.219E+03
4 RPP -1.722E+03  1.722E+03 -1.722E+03  1.722E+03 -3.048E+02  1.341E+03

MODE N
IMP:N 1 1 1 1 0
SDEF POS = 0 0 2.000E+02 PAR = 1 ERG = D1 WGT = 1.76191 E+14
SI1     1.52000E-07 4.14000E-07 1.13000E-06 3.06000E-06 8.32000E-06
        2.26000E-05 6.14000E-05 1.67000E-04 4.54000E-04 1.24000E-03
        3.36000E-03 9.12000E-03 2.48000E-02 6.76000E-02 1.84000E-01
        3.03000E-01 5.00000E-01 8.23000E-01 1.353      1.738
        2.232      2.865      3.68       6.07       7.79
        10         12         13.5       15         17
SP1      0.000000000 1.16366E-06 3.26288E-06 1.17775E-05 2.94437E-05
        3.66281E-05 7.82247E-05 1.37112E-04 2.84469E-04 6.16246E-04
        8.02362E-04 1.79781E-03 1.40701E-03 3.33691E-03 5.01139E-03
        4.44130E-03 7.36328E-03 6.91172E-03 1.07663E-02 8.47806E-03
        7.17972E-03 5.16656E-03 4.42066E-03 6.66341E-03 1.46639E-03
        5.63366E-04 4.72692E-05 3.66336E-05 1.22548E-05 4.29716E-06
FMESH4:N  ORIGIN -1.559E+03 -1.559E+03  1.219E+03
        IMESH 1.559E+3 IINTS 100
        JMESH 1.559E+3 JINTS 100
        KMESH 1.219E+3 KINTS 1
FS4N    2.000E+02 0 2.000E+02 5.0
E0      1.52000E-07 4.14000E-07 1.13000E-06 3.06000E-06 8.32000E-06
        2.26000E-05 6.14000E-05 1.67000E-04 4.54000E-04 1.24000E-03
        3.36000E-03 9.12000E-03 2.48000E-02 6.76000E-02 1.84000E-01
        3.03000E-01 5.00000E-01 8.23000E-01 1.353      1.738
        2.232      2.865      3.68       6.07       7.79
        10         12         13.5       15         17
EM0     4.47217E-17 4.82200E-17 6.14000E-17 1.33001E-16 2.20127E-16
        3.63004E-16 6.00790E-16 9.95378E-16 1.65009E-15 3.10578E-15
        7.37100E-15 2.76533E-14 1.46000E-13 6.60300E-13 4.09700E-12
        8.37400E-12 2.42000E-11 4.74240E-11 1.09629E-10 1.22693E-10
        1.69923E-10 3.07239E-10 7.76918E-10 2.63932E-09 1.71797E-09
        2.63410E-09 3.21000E-09 3.02790E-09 3.80600E-09 4.60000E-09
FM5     1
M1      001001.80 0.16
        006018.80 0.57
        013027.80 0.06
        014000.80 0.19
M2      007014.80 0.7699
        008016.80 0.2102
M3      001001.80 0.1049
        006018.80 0.6843
        011023.80 0.0140
        012000.80 0.0019
        013027.80 0.0319
        014000.80 0.2108
        016000.80 0.0092
        020000.80 0.0399
        026000.85 0.0041
MODPT F 30
NPS 100000
```

```
Empty Model w/ ICRU 44 Response & 10000 g/Li Leakage (Neutron, Multi Adjoint)
1 1 -1.70E+0 -1  4
2 2 -1.22E-3 -2  4
3 2 -1.22E-3 -3
4 3 -2.34E+0  3 -4
5 0 1 2

1 RPP -2.286E+03  2.286E+03 -2.286E+03  2.286E+03 -8.000E+02  0.0000000
2 RPP -2.286E+03  2.286E+03 -2.286E+03  2.286E+03  0.0000000  1.524E+03
3 RPP -1.800E+03  1.800E+03 -1.800E+03  1.800E+03  0.0000000  1.219E+03
4 RPP -1.722E+03  1.722E+03 -1.722E+03  1.722E+03 -3.048E+02  1.341E+03

MODE N
IMP:N 1 1 1 1 0
SDEF POS = 2.000E+02 0 2.000E+02 PART=1  ERG=01 WGT=1.76181E+14
SI1      1.82000E-07 4.14000E-07 1.13000E-06 3.06000E-06 8.32000E-06
         2.26000E-05 6.14000E-05 1.67000E-04 4.54000E-04 1.24000E-03
         3.36000E-03 9.12000E-03 2.48000E-02 6.76000E-02 1.84000E-01
         3.03000E-01 5.00000E-01 8.23000E-01 1.353      1.738
         2.232       2.865       3.68        6.07       7.79
         10          12          13.5        15         17
SP1       0.000000000 4.82000E-17 8.14600E-17 1.33881E-16 2.20127E-16
         3.63804E-16 6.00750E-16 9.95378E-16 1.66666E-15 3.10578E-15
         7.37100E-15 2.78639E-14 1.48036E-13 8.80360E-13 4.86766E-12
         8.37480E-12 2.42008E-11 4.76240E-11 1.09286E-10 1.22883E-10
         1.69923E-10 3.07239E-10 7.76915E-10 2.63932E-09 1.71797E-09
         2.63410E-09 3.21000E-09 3.02780E-09 3.60000E-09 4.60000E-09
FMESH4:N  ORIGIN -1.500E+03 -1.500E+03 1.500E+02
         IMESH 1.500E+3 IINTS 100
         JMESH 1.500E+3 JINTS 100
         KMESH 2.001E+2 KINTS 1
         EMESH 17
FS4N     0 0 2.000E+02 5.0
E0       1.82000E-07 4.14000E-07 1.13000E-06 3.06000E-06 8.32000E-06
         2.26000E-05 6.14000E-05 1.67000E-04 4.54000E-04 1.24000E-03
         3.36000E-03 9.12000E-03 2.48000E-02 6.76000E-02 1.84000E-01
         3.03000E-01 5.00000E-01 8.23000E-01 1.353      1.738
         2.232       2.865       3.68        6.07       7.79
         10          12          13.5        15         17
EM0      3.07697E-07 1.16366E-06 3.28288E-06 1.17775E-05 2.94437E-05
         3.65281E-05 7.82247E-05 1.37112E-04 2.84469E-04 6.10245E-04
         8.62992E-04 1.78781E-03 1.40701E-03 3.33981E-03 5.81166E-03
         4.44130E-03 7.36328E-03 6.91172E-03 1.07863E-02 8.47805E-03
         7.17972E-03 6.16669E-03 4.42666E-03 6.86341E-03 1.49839E-03
         5.63068E-04 4.72690E-05 3.88339E-05 1.22549E-05 4.20719E-06
FM5      7.82922E-07
M1       001001.80 0.16
         006016.80 0.57
         013027.80 0.06
         014000.80 0.19
M2       007014.80 0.7666
         008016.80 0.2102
M3       001001.80 0.1049
         006016.80 0.8943
         011023.80 0.0140
         012000.80 0.0010
         013027.80 0.0319
         014000.80 0.2109
         016000.80 0.0092
         020000.80 0.0399
         026000.55 0.0041
MOOPT A 30
CUT:N J 17
NPS 100000
```

VITA

Zia Tompkins was born on 29 November, 1979, in Montreal, Canada, but considers Jessup, Maryland, home. Zia graduated from Archbishop Spalding High School, class of 1998 and attended Naval Nuclear Power School in Charleston, SC. Zia entered the University of Maryland and graduated with a triple-degree quadruple major in Physics, Nuclear Engineering, Pure Mathematics and Chemistry. Zia worked as a consultant with Gamma Engineering before coming to the University of Tennessee where he now pursues a triple masters' in Physics, Nuclear Engineering and Aviation Systems. Zia is an avid flyer of Cessnas and other small piston aircraft and enjoys the occasional trip to the beach.